
DEDICATED TO THE 90TH
ANNIVERSARY OF IGEN RAS

Seismogenic Nature of Fluid-Dynamic Structural Parageneses of the Uryakh Gold Ore Field (Northeastern Transbaikalia)

T. M. Zlobina^{a, *}, V. A. Petrov^{a, **}, V. Yu. Prokofiev^a, S. S. Abramov^a,
A. A. Kotov^a, A. A. Wolfson^a, and A. B. Leksin^a

^a*Institute of Geology of Ore Deposits, Petrography, Mineralogy and Geochemistry,
Russian Academy of Sciences, Moscow, 119017 Russia*

*e-mail: tatiana1946@yandex.ru

**e-mail: vlad243@igem.ru

Received June 19, 2018; revised March 21, 2019; accepted April 25, 2020

Abstract—New data on the geological structure and ore-bearing structural parageneses of the Uryakh gold ore field are presented. The formation of the deposit occurred in dynamic shear regime along ore-controlling deep-seated faults of the Syulban fault system and faults of the system transverse to it. The interaction of two duplex shear systems resulted in the block structure of the ore field. Tectonophysical methods have established the individual development of tectonic blocks during the period of gold-bearing fluid input in a seismically active regime. The specific features of the formation of ore-bearing fracture–fault structural parageneses in the blocks resulted from the change in the seismic regime under the action of pressure and gas-saturated fluids. The parameters of the fluid system were determined by fluid inclusion studies in quartz. An unstable variable compression–extension regime of the early phase of seismic activity led to the formation of hybrid structural parageneses under the influence of stresses of damping shear and injective hydrodynamic stress. Variations in the stress–strain state of the medium in this phase correspond to a transient seismic regime and are consistent with variations in the thermobarometric parameters of the fluid system. In the late phase of seismic activity, a stable uniaxial tension regime with a superlithostatic fluid pressure occurred, which caused brittle deformations independent of slip along the fault. The centroid mechanism of such deformations, which is rarely found in the dynamic regimes of hydrothermal deposits, ensured the formation of structural parageneses unusual for shear zones, which resulted in a different combination of structural and morphological types of orebodies in the blocks.

Keywords: structure, structural paragenesis, fluid–dynamic structural parageneses, ore field, orebodies, veins, seismic regime, tectonophysics, fluid dynamics, stress–strain state of the medium, fluid migration

DOI: 10.1134/S1075701520040066

INTRODUCTION

Mesothermal hydrothermal gold deposits located in orogenic belts along the convergent margins of lithospheric plates are included in the orogenic class. They include the Uryakh gold ore field, localized in the Syulban zone of ancient deep-seated faults, extending along the Proterozoic Baikhalides at the boundary with the Siberian Craton (Figs. 1a, 1b). Views on the structural control of orebodies have repeatedly changed throughout the history of studying the structure of the Uryakh gold ore field. The general Syulban fault was unequivocally perceived as a fluid-supplying and ore-controlling structure. Its tectonic activity in the reverse-fault regime was explained (Kucherenko and Gavrillov, 2011, 2012) by the formation of a structural paragenesis of steep shear fissures and gently dipping extension fissures that hosted veins and vein–stringer zones with linear morphology. The formation of veins with a sigmoid morphology was

explained by a fold control reflected on the structural and lithological map of the ore field (Korzhet al., 1976unpub¹). During exploration, conclusions about the control of orebodies in large fold shapes were not confirmed. The reverse-fault regime along the Syulban fault was also discussed, with which the formation of thrusts was paragenetically associated (Molodtsov et al., 2008unpub²). However, none of the known models (Sylvester, 1988; Woodcock and Fischer, 1986;

¹ Korzh, V.V., Anikin, V.A., and Bolshedvorsky, K.A., Structural–Lithological Map of the Uryakh Ore Field, Scale 1 : 10000, Report of the Irkutsk Geological Survey Expedition of Irkutsk State University on Geological Surveying for Ore Gold. Foundations of Mingeo of RSFSR, Glavvostokgeologiya, 1976.

² Molodtsov, I.V., Baranov, V.N., Mavrichev, V.G., Kameneva, L.A., Petrukhina, I.P., and Vinogradov, A.E., High-Precision Integrated Airborne Geophysical Surveys (Aeromagnetometry, Gamma Spectrometry) on scale of 1 : 10000 at the Uryakh Ore Field. Report of SPE Geological Survey. St. Petersburg, 2008. 126 p.

Ramsay and Huber; 1987; Riedel, 1929) explained the formation of the entire observed complex of structural elements in the paragenesis with inferred slips along the fault. In addition, we drew attention to development in the fault zone of numerous dilatation microstructures of the crack–seal inclusion bands, usually formed in a seismic regime.

At present, copious data have accumulated that the migration of ore-forming fluid flows from source in the field of mineral formation carried out during periods of seismic activity of fluid-conductive faults (Cox, 1995, 2005, 2016; Sibson et al., 1988; Nguyen et al., 1998; Petrov et al., 2008). Earthquakes with hypocenters at different depths in a conducting fault can open fluid reservoirs of different nature and ensure mixing of fluids and their movement through permeable channels in the sphere of mineral formation. After a major earthquake (mainshock), the depth of the boundary of brittleness–plasticity of rocks drops sharply (Cox, 2005; Sibson, 2004; Petrov, 2011). Cascades of subsequent weaker aftershock sequences create a highly dynamic system, in which all processes are interrelated—geochemical; magmatic-metamorphic alteration of the medium and fluid composition; pressure fluctuations of fluid systems; brittle fracture and dilatancy expansion of rocks. Research of the chemical and isotope compositions of the ore-forming fluids of seven Russian mesothermal gold deposits (Bortnikov, 2006; Bortnikov et al., 1996, 1998, 2004; Bortnikov et al., 1999; Prokof'ev et al., 2010; Vikent'eva et al., 2017) showed that the ore formation processes involve solutions, magmatic-metamorphic fluids, and meteoric water. With the joint development of seismogenic destruction processes and migration of pressure fluids containing gases and saline solutions, repeated pressure release and degassing of fluid systems occur. Degassing of a fluid system in turn disrupts the ratio of gas concentrations (C_2/CH_4) regulating the pH of solutions, and decompression boiling of fluids increases the salt content in solutions (Zlobina et al., 2017). Elevated concentrations in salt solutions reduce the critical failure parameters and accelerate the for-

mation of fissures, which under decompression conditions quickly fill with fluids.

The aim of the paper is to study the processes involved in the formation of the structure of the Uryakh gold ore field and the formation mechanisms of the ore-bearing structural parageneses employing the seismogenic concept of deposit formation.

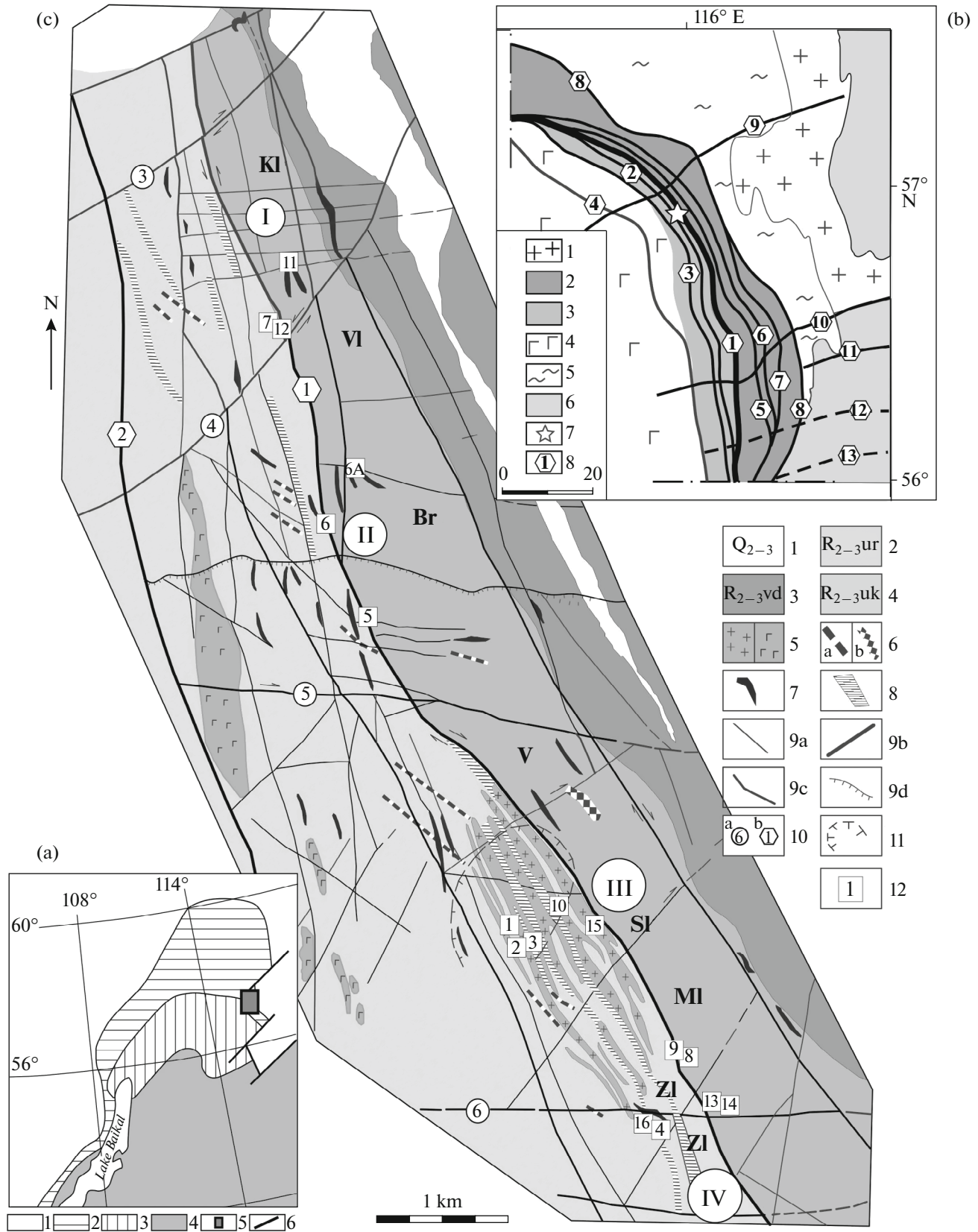
STATE OF THE PROBLEM

The concept of hydrothermal deposit formation in a seismic regime appeared by chance in studying mesothermal gold deposits. One problem is the permeability of faults in the mesothermal depth range, and another is assessing the effect of fluid pressure on paleofracture processes.

The regime of fluid flow migration in a fault explains the fault-valve model (Sibson, 1981; Sibson et al., 1988), which regulates pulsed fluid flow during a cycle of seismic events. The model takes into account the relationship between the pore and lithostatic pressure, as well as the volume of fluids entering the active fault. When the seismic stress exceeds the lithostatic pressure in the area of hydrothermal source generation, the “valve is open” for active upward fluid migration. As the volume and pressure, which exceeds lithostatic, of the hydrothermal solutions increase, the active migration of fluids continues, and when the pressure is released as a result of seismogenic destruction, the flow activity decreases. In the intervals between seismic events in fissures filled with fluids, minerals are deposited that “block” the fissures and lower the permeability decreases—the valve closes. Dilatation microstructures of the “crack–seal inclusion bands” type reflect multiple cycles of “pumping” and depressurizing of the fluid during the evolution of the conducting fault (Cox, 1995, 2005).

Experiments on injecting water into wells under pressure in low-permeable rocks with and studying the styles of seismic sequences (aftershock and/or swarm) with high hydrothermal activity allowed Cox (2016) to give preference to the fluid-injected swarm earthquake

Fig. 1. Geological–tectonic position (a, b) and geological–structural scheme of Uryakh ore field (c). (a) Geological–tectonic position (after (Mitrofanov, 2006) with additions). (1) Siberian Craton (SC), (2) Baikal-Patomsky belt; (3) Baikal-Muya belt (BMB); (4) Barguzin superterrane; (5) inset shown in (b); (6) regional faults. (b) Geological–tectonic scheme of transition from BMB to western margin of Siberian craton (modified after Karasev (2009)). (1) granitoids PZ₃; BMB; (2) metamorphosed sedimentary terrigenous rocks PR₂₋₃; (3) metavolcanics PR₂₋₃; (4) intrusive rocks PR₂₋₃; SK; (5) gneiss granites PR₁, tectonized; (6) metamorphosed rocks AR; (7) position of Uryakh ore field; (8) faults. Syulban system (1–8): (1) Syulban; (2) Vodorazdelny; (3) Karalon; (4) Ust-Karalon; (5) Verkhne-Uryakh; (6) Orlov; (7) Verkhne-Talainsky; (8) Malokudinsky; Kodar-Chinei system (9–13): (9) Vitimsky; (10) Talain (Kodar); (11) East Syulban; (12) Chinei-Wakatsky; (13) Namarakitsky. (c) Geological and structural scheme (based on geological and structural map with scale of 1 : 10000, made in ARCGIS system at I GEM RAS, using: (Korzh et al. 1977; Cherepanov and Goncharuk, 1982f; Molodtsov et al., 2008f; Danilyuk et al., 2009f). (1) Quaternary deposits; (2–3) metamorphosed terrigenous–carbonate rocks of Ust-Uryakhaya, R_{2-3ur} (2) and Vodorazdelny, R_{2-3vd} (3) formations; (4) metavolcanic rocks of Ust-Kelyansk sequence, R_{2-3uk}; (5) intrusive rocks of Talain complex, R_{2-3t}; gabbroids (ГГ), granitoids (+); (6) minor Paleozoic intrusions (dikes): Kadali Butui, PZ_{3kb} (a) and Kachoisky, PZ_{3k} (b) complexes; (7) Q–Au veins; (8) beresitization zones; (9) tectonic faulting: fissure (a), ore supply (b), ore distribution (c), thrust (d); (10) faults (slip of ore period); (a) first-order of Syulban system: (1) Syulban, (2) Vodorazdelny; (b) second-order of transverse system: (3) Klimovsky; (4) Valunny; (5) Pravy Barachny; (6) Yuzhny; (11) zone of increased fluid permeability; (12) structural measurement sites and their numbers. Sectors of ore field: Kl, Klimovsky; Vl, Valunny; Br, Barachny; V, Vetvisty; Sl, Sulfide; Ml, Malachite; Zl, Zolotoi. Tectonic blocks: I, Klimovsky; II, Valunny–Barachny; III, Stockwork; IV, Yuzhny (I, II, III, IV, also numbers of segments of Syulban fault).



model. Cascades of earthquake swarms with low magnitudes (<4) “start” in faults with fluid volumes from 10^4 to 10^5 m³, flowing at a rate of at least several tens of liters per second. Propagation of the seismic front at a speed of several hundred meters per day causes extensive dilatancy. According to the Coulomb criterion, for $\sigma_{\max} - \sigma_{\min} > 5.7T$, deformations in the fault zone occur in response to the increased pressure from the fluid pressure, and for $\sigma_{\max} - \sigma_{\min} < 4T$ (Griffith criterion), dilatancy fissuring near a conducting fault can begin before shear deformation on the fault. Groups of microearthquakes of the same type (multiplets) contain up to several tens of events of the same type. Cox (2016) considered the development of each multiplet with a study of crack–seal inclusion structures in a stratified vein or in metasomatites, as an asperity characterizing acts of microfracturing with the same heterogeneity.

The impact of seismotectonic processes on pulsed fluid migration was considered in a gradient field with varying PT parameters. The brittle–ductile transition zone is estimated (Cox, 2005; Sibson, 2004) as abnormally low-permeable, delimiting regions where the hydrostatic fluid regime changes to superhydrostatic or nearly lithostatic. The presence of several layers of low-permeable rocks leads to abnormal increases in hydrostatic pressure (fluid overpressure) with depth, up to equalization with the lithostatic pressure at higher levels relative to the critical zone (20–25 km) of the gradient field (Cox, 2005). In the changing PT regime of the gradient field, permeability of tectonic conductors and formation of fracture architecture of the fault zone were studied (Sibson et al., 1988; Cox, 1995; Sibson and Skott, 1998; Petrov et al., 2008; Petrov, 2011).

The principal strain diagram proposed by (Cox, 2016), shows how changes in fluid pressure and/or the stress state can lead to the formation of fracture structural parageneses of various genotypes. Under a significant excess of lithostatic pressure over the hydrostatic pressure of fluids, brittle failure in the fault zone is caused by high deviatoric seismic compressive stress, which triggered slip along the fault. As stress relaxes and the hydrostatic pressure of fluids increases, a paragenesis of hybrid fissures occurs, associated both with slip along the fault and fracturing under the influence of fluid pressure. When the hydrostatic pressure approaches the lithostatic (up to equalization of their values), brittle fracture prevails solely under the impact of a pressure pulse from the fluid flow. For low stresses ($\sigma_1 - \sigma_3 < 4T$, where T is the yield strength) and hydrostatic pressure significantly exceeding the lithostatic pressure, fissure paragenesis occurs under tension conditions influenced by the increased fluid pressure. We attribute the aforementioned (Cox, 2016) seismogenic paragenesis as fluid-dynamic.

The influence of abnormally excess fluid pressure on rock failure was considered by (Sibson, 2004; Cox

2005, 2016) with studies on the formation of gold deposits in low-magnitude (<4) earthquake conditions. The Uryakh ore-forming system developed in a zone of intense seismicity, which is characterized (Vertlib, 1997) by the frequent occurrence of earthquakes with magnitudes $M > 5$ and by subsidence of the base of the seismogenic zone to a depth of 30 km. In such a seismogenic fracture setting, frequent pressure drops in the fluid system do not contribute to anomalous hydrodynamic pressure, and changes in the dynamic regimes of all interacting systems that influence the formation of structural parageneses are unpredictable. The impact of earthquake mechanisms, depending on the structure of the unloading of earthquake foci in a wide range of depths in the seismogenic zone, on hydrodynamic processes and the formation of structural parageneses are important for the Uryakh system and have not been previously considered.

RESEARCH METHODS

In the zone of influence of the Syulban fault, in a strip 4 km wide and 12 km long, special structural mapping of tectonites was carried out with mass measurements of the azimuthal parameters of structural elements, by collecting samples for thermobarogeochemical studies of the fluid system. A detailed study of metamorphic and metasomatic rock alterations was carried out using the pseudosectional method (Connolly and Pettrini, 2002) and a chlorite–sericite thermobarometer (Vidal et al., 2007). Cartographic materials were analyzed in the ARCGIS environment: structural–lithological survey (Korzhanov et al., 1976unpub); geophysical surveys—gamma-ray spectroscopy, resistivity survey, high-precision magnetic survey (Danilov et al., 2008unpub³; Molodtsov et al., 2008unpub). To reconstruct the macrostructure, we used model-based structural-paragenetic analysis methods (Riedel, 1929; Rastsvetaev, 1987; Sylvester, 1988). In solving problems of the mutual influence of tectonodynamic and fluid systems, the results of tectonophysical and thermobarogeochemical research are of particular importance.

Methods for Studying the Stress–Strain State of the Medium

In the long history of the tectonic development of the area, deformations corresponding to the period of input of ore-bearing fluids were selected by reconstructing the principal normal stress vectors (σ_1 , σ_2 , σ_3) and collinear strain vectors (A, B, C) along conju-

³ Danilov, A.A., Molchanov, V.I., Lyashchenko, N.G., Khokhlov, N.A. etc., Information report on the results of prospecting–appraisal and exploration work at the Uryakh ore field for 2008 M.: Federal State Institution Scientific and Research Enterprise Rosgeofond, 2009. Book 1. 113 p; Book 2. 51 p; Book 3. 27 p.; Book 4. 35 p.

gate tangential shear surfaces (Gzovsky, 1975), determined from indicator minerals of the ore process. Based on mass measurements of conjugate pairs of ore veins at mineralization sites (see Fig. 1c), numerous orientations of vectors A, B, C were reconstructed, the exit of which to the upper hemisphere of the Schmidt grid are reflected on spherograms as distribution density isolines (in %). The vector scattering measure was estimated from axial-type parametric statistics (Bingham, 1974) with elliptically shaped confidence intervals, also in %. For a quantitative estimate of the change in the stress using tectonophysical methods, usually, the elongation (shortening) coefficients of vectors σ_1 , σ_2 , σ_3 (hereinafter, $\sigma_1 < \sigma_2 < \sigma_3$) are applied, which are calculated in different ways. In fact, such coefficients, with values from -1 to $+1$, determine the shape of the strain ellipsoid, a virtual tool allowing one to assess the strain regime in a changing stress field. In kinematic methods (Gushchenko, 1979; Angelier, 1975), the Lode–Nadai coefficient (μ) is used, under the condition that the directions of the tangential stress vectors are known, which are determined by slickenlines. However, in hydrothermal deposits, the multiple “healing” of early and intraore slickenlines during the fluid supply period turns these planes into slickensides, from which it is not always possible to reconstruct the direction of slip and tangential stresses. Therefore, when studying the Uryakh gold ore field, a different approach was used to calculate the coefficients by the method of (Bingham and Mardia, 1978). The following parameters were calculated: t_1 , t_2 , t_3 of the Bingham distribution, which reflects the preferred directions of action of the principal normal stresses, each of which corresponds to an eigenvalue of the tensor matrix. Such numbers, having values from -1 to $+1$, can be used to estimate the relative change in vectors σ_1 , σ_2 , σ_3 , respectively, in directions t_1 , t_2 , t_3 . In addition, the coefficients k_1 , k_2 , k_3 of the asymmetry of tensors are calculated (Bingham and Mardia, 1978). The method (Zlobina, 1991) was also applied for classifying ore-hosting fissures paragenetically related to slip along a fault. The relationship of a particular system of fissures with a certain slip along a fault was established from estimates of the ratio of the determinants of the deviator tensors $\text{Det}(M_{i,j})/\text{Det}(M_{x,y})$, characterizing the isometric position on the sphere of fault planes and fissure systems in the basic coordinate system. Geometric analysis of fault projections on a stereographic grid with respect to changing orientations of maximum σ_3 (vector C) and minimum σ_1 (vector A) compression and, taking into account estimates of changes in the *stress–strain state* (SSS) of the medium, it is possible to determine the change in the type of slip during continuous deformation (e.g., transtensional shear or shear transforming into shear–thrust).

Methods for Studying the Fluid System

Estimates for the fluid system parameters were obtained in fluid inclusion (FI) studies in gold-bearing vein quartz trapped during mineral formation. Among the studied FI, in accordance with the criteria of (Roedder, 1984), primary, primary–secondary, and secondary FI were distinguished. Primary fluids include FI uniformly distributed in the bulk of the host mineral or confined to growth zones, and secondary fluids are confined to cross-cutting host-mineral fractures. Microthermometric FI studies were performed with measuring equipment comprising a THMSG-600 Linkam microthermal stage (England), an Olympus microscope (Japan), a video camera, and a control computer. The equipment allows real-time measurements of the phase transition temperatures in the range from -196 to 600°C , to observe them at high magnifications, and to obtain digital micrographs. The salt concentration for FI was calculated from the melting temperature of ice using data from (Bodnar and Vityk, 1994). The salt composition of the solutions was determined by the eutectic temperatures (Borisenko, 1977). Pressure was estimated for assemblages of syngenetic inclusions of types 1 and 2 of heterogeneous fluid as the pressure of saturated water vapor. The salt concentrations and water vapor and carbon dioxide pressures were estimated using the FLINCOR program (Brown, 1989). A gross analysis of the composition of inclusion fluids was carried out from charges of 0.7 g of the $-0.5 + 0.25$ mm class of monomineral quartz fractions at the Central Research Institute of Geological Prospecting for Base and Precious Metals (analyst Yu.V. Vasyuta) according to the method (Kryazhev et al., 2006). FI in quartz were thermally exposed at 500°C . Gas chromatography (TsVET-100 chromatograph) was used to determine the amount of water to calculate the concentration of elements in the hydrothermal solution. Carbon dioxide, methane, and hydrocarbons were also analyzed. After preparation of aqueous extracts in solution using ion chromatography (TsVET-3006 chromatograph, sensitivity 0.01 mg/L), Cl, SO_4 , and F were determined; ICP MS (Elan-6100 mass spectrometer) was used to determine K, Na, Ca, Mg, and other elements.

TECTONIC POSITION, GEOLOGICAL STRUCTURE, AND FORMATION CONDITIONS OF THE URYAKH GOLD ORE FIELD

The Uryakh gold ore field is confined to the Syulban deep fault system, which trends arcuately NNW (Figs. 1a, 1b), extending along the outer part of the eastern segment of the Baikal–Muya belt (BMB) and the margin of the Siberian Craton. It is located on the southeastern flank of the Karalon–Mamakan geosubstructure of the BMB and is part of the Tallai–Oryol polymetal–gold placer zone with total resources of more than 400 t of gold (Mitrofanov, 2006). The ore

zone includes, in addition to Uryakh, large gold ore fields (Bakhtarnak, Karalon, Nizhny Orlov, Orlov) and small and medium-sized deposits. For the eastern segment of the BMB, Rytsk et al. (2011) developed geodynamic models of the marginal–continental and island–arc formation of the Proterozoic neocrust in the setting of Early and Late Baikalian collisional tectonic cycles. The Karalon–Mamakan geostructure was formed in the Late Baikalian tectonic cycle. Later, Rytsk et al. (2018) admitted the “synshear rifting” model, and the regional geological position of the Tallai–Oryol ore zone is determined by shear structures at the boundary of the eastern segment of the BMB and the Siberian Craton. In the central part of the ore zone, the Muya–Chara wall is the transitional region from the BMB to the craton. Here it was established (Karasev, 2009) that ENE-trending ancient faults of the Kadar–Chinei system are bounded by modern rift-related embryonic structures of the margin of the Siberian Craton, which are principal seismogenic structures of the region. In the ARCGIS environment, we carried out procedures for combining cartographic materials (Karasev, 2009; Korzh et al., 1976unpub) and refined the fault location points of the Syulban and Kodar–Chinei systems (see Fig. 1b). According to the data of (Molodtsov et al., 2008unpub), within the Uryakh ore field, the Syulban fault is expressed as a contrasting gravitational step (a negative gravity anomaly of -7 mGal) and a complexly differentiated magnetic field. Such data are consistent with those of (Wertlib, 1997) about the great depth of the base of the crustal seismogenic zone and confirm the complex tectonic position of the Uryakh ore field at the orogen–craton boundary at the junction of submeridional and sublatitudinal deep faults.

Host Rocks, Morphogenetic Features of Orebodies, and Ore Composition

The orebodies of Riphean metavolcanites of mafic, intermediate, and felsic compositions of the Ust–Kel–yan sequence (R_{2-3uk}), widespread to the west of the Syulban fault, as well as rocks of the calcareous–shale terrigenous complex of the Ust–Uryakh (R_{2-3ur}) and Vodorazdelny (R_{2-3vd}) formations, widespread to the east of it (see Fig. 1c). Rocks of the intrusive syntectonic gabbro–diorite–plagiogranite Tallai complex (R_{2-3t}) with a plagiogranite age (Rytsk et al., 2011) of 604 ± 7 Ma and gabbroid age of 625 ± 14 Ma are widespread west of the Uryakh ore field. Small gabbroid bodies are traced on its western flank (see Fig. 1c) along the Vodorazdelny fault. The intrusive rocks of the granitoid series are widespread both in metagabbroids on the northwestern flank of the ore field and in the sequence of metavolcanites in the central and southern parts. Paleozoic intrusions are represented by dikes of the Kadali Butui (PZ_3kb) and Kachoi (PZ_3kc) complexes. According to structural mapping data, the spatial distribution of all dikes in shear faults

of three systems has been categorized: northwestern–submeridional, consistent with the trend of the Syulban fault, sublatitudinal and northwestern (diagonal). The first two systems of shear surfaces also contain orebodies, and faults of the third system do not control the placement of orebodies. In faults of the diagonal system, dikes, mainly dolerite–diabase of the Kadali–Butui complex, are often subjected to beresitization.

The bodies of economic ores of various structural and morphological types (vein, bulk stockwork, linear stockwork) are localized in the vertical depth range of 0–800 m. They are represented by quartz–gold ore with silver veins; vein–stringer zones, often accompanied by disseminated ore mineralization; as well as independent bulk and linear stockwork ore zones. The vein zones, with a length of 0.2 to 3.3 km and thickness of 3.5 to 20 m, are controlled by tectonic faults, consistent with the trend of the Syulban fault. Individual veins lying in tectonic faults with different strike and dip have different thicknesses (from 1 to 5 m) and morphologies. Stringer–disseminated mineralization is prevalent mainly in the shallow zones of beresitized rocks and is localized in quartz–carbonate metasomatites of the Main Suture of the Syulban fault. The thickness of quartz stringers is from 1–5 to 10 cm.

The main minerals of economic ores are gold (native and mineral complexes), silver (native and complexes), acanthite–argentite, and fahlore (Cherepanov and Goncharuk, 1982unpub⁴). Sulfide ore mineralization is represented mainly by pyrite, chalcopyrite, sphalerite, galena; less frequently, by arsenopyrite and pyrrhotite. Gold and silver tellurides were noted; scheelite and molybdenite were also observed. The mineral base of the veins consists of quartz and carbonates. In orebodies, an extremely uneven distribution of gold and silver is observed (Cherepanov and Goncharuk, 1982f). Overall, the total amount of sulfides in enriched areas, amounting to 0.5–2.5%, makes it possible to attribute the Uryakh gold ore field as a low-sulfide quartz–gold–silver formation.

Evolution of the Syulban Fault Zone

Excessive stresses of collisional near-latitudinal regional compression in the Proterozoic are indicated by compaction (shortening) in the direction of compression of the substrate of the geomedium, the formation of folded anti- and synforms of longitudinal flexure in the terrigenous sequence, as well as the formation of the Syulban fault plane, curvilinear both in plan view and profile. This is confirmed by the results of structural mapping of the Uryakh ore field. The sharp contiguity of the central faults (1, 2, 5) of the Syulban system was established, located near the contact of rocks with different rheological properties (see

⁴ Cherepanov, V.K. and Goncharuk, S.G., Report on Prospecting Works of the Syulban Party within the Uryakh Ore Field (ore gold) for 1979–1981. Funds of Irkutsk TSU, Irkutsk, 1982.

Fig. 1b). The axial plane of a large anticlinal fold, the western limb of which adjoins the eastern side of the Syulban fault, has a submeridional strike. The Syulban fault plane changes its orientation from west to east both in dip and strike. The transpressional regime along the faults of the Syulban system in PR₂ is determined by structural features of shear in gneiss granites (PR₁) along faults 9 and 10 (see Fig. 1b) of the Kodar-Chinei system. The development of second-order faults 3–6 (see Fig. 1c) of sublatitudinal and northeastern strike transverse to the orientation of the megastructure is paragenetically related to the shear slip along faults 9 and 10. In the Late Paleozoic, the tectonic regime changed. Cases of low-amplitude shear of dikes of the Kadali-Butui complex in the sublatitudinal direction and small thrust displacements from north to south with a sublatitudinal shear component are noted, which indicates a Late Paleozoic shear–thrust fault regime of two fault systems: the main Syulban and the the ENE-trending fault system transverse to it. When the two systems were activated in the Proterozoic and Paleozoic, the Syulban megastructure was divided into tectonic blocks corresponding to segments I, II, III, and IV (see Fig. 1c).

We attribute the metamorphic regional alterations of rocks of the Syulban fault zone to greenschist facies. The pseudosection method (Connolly and Petrin, 2002; Perplex 6.7 software) yielded the maximum *PT* parameters of greenschist rock alterations: *P*, 4.4–4.5 kbar; *T*, 300–420°C. In various activation phases of the Syulban fault in wallrocks and its sutures, polychronous and unevenly diverse tectonites were formed. In the process of preore dynamic metamorphism, rocks were altered into mylonites and schists. We attributed the mylonites to the dynamic metamorphism products according to the tectonic–facies features of the classification of (Patalaha et al., 1987). In the western limb, they are traced on small segments in bends of the fault, where their thickness varies from 80–120 m in segment II to 120–140 m in segment III. The mylonitization zones are the longest in the eastern limb of the fault, with a thickness reaching 130 m in segment IV and increasing to 310–360 m in segments I and III.

Tectonomagmatic activity in the Proterozoic and Paleozoic was accompanied by syntectonic polychronous metasomatism. The earliest preore metasomites are quartz–carbonate, which formed in the dolomitization of mafic rocks and albitization–dolomitization (with rutile and monazite) of felsic rocks, which healed the Main and Eastern sutures of the Syulban fault (Figs. 2a, 2b, 2d). The distribution of such metasomatites, sufficiently uniform in composition, in the fault sutures to a depth of 1 km is confirmed by geophysical data (Fig. 3). These rock alterations are followed by the syntectonic development of blastomylonites and cataclases. In neighboring segments of the Syulban fault (see Figs. 1c, 2), different degrees of

destruction of quartz–carbonate metasomatites and mylonitization and cataclasis of wallrocks of the Main suture were observed. Whereas in segments II and IV only prismatic cataclasis, schistosity, and linear plicature are noted, and mylonitization of wallrock is widespread with relatively good preservation of quartz–carbonate metasomatites (see Figs. 2a, 2b), segments I and III feature near-fault comminution and boudinage of quartz–carbonate metasomatites (Figs. 2c, 2d). These indicate the autonomous development of tectonic blocks after the early stage of metasomatic rock alteration. Beresitites are the product of the late synore metasomatic rock alteration. They developed not only as a near-vein alteration in the host rocks, but also in areas with increased fracturing. Linear beresitization zones, with a strike matching the Syulban fault, are more widespread in metavolcanites than in schists.

In the process of syntectonic polychronous metasomatism of protoliths of felsic and mafic–intermediate composition, mylonites are altered to sericite–carbonate–rutile and sericite–carbonate–chlorite blastomylonites, respectively. In the granitoid distribution areas in volcanic rocks, metasomatites containing tourmaline and fuchsite (Cr₂O₃ 1.5–2 wt %) conformable with schistosity were observed. These minerals are present in narrow local recrystallization zones of previously formed sericite–albite–chlorite–carbonate–rutile metasomatites. The data obtained by the method of (Vidal et al., 2007, “chlorite–sericite thermobarometer”) indicate that blastomylonites of the same type in terms of the development of the metasomatic process in all segments of the Syulban fault zone formed at very high pressures of 6 kbar at temperatures of 250–300°C, whereas beresitization of Paleozoic mafic dikes took place, according to the data obtained by the same method (Vidal et al., 2007), under close temperature conditions of 270°C, but with a drop in pressure to 2.2 kbar. It was also established that with the beresitization of early sericite–albite–chlorite–carbonate–rutile metasomatites, the composition of newly formed carbonates becomes more magnesian. According to the results of the study of metasomatites, it was concluded that iron–magnesian–carbonate is overprinted on carbon dioxide metasomatism; however, the reason for the large drop in pressure was unclear. According to the results of isotope–geochronological studies by the Rb–Sr and ⁴⁰Ar–³⁹Ar methods (Chugaev et al., 2015) of near-vein beresites that developed over carbonaceous schist, the formation of synore metasomatites occurred in the period 281–276 Ma.

In the distribution areas of vein zones and ore stockworks of the Uryakh ore field, a structural–paragenetic analysis of near-fault fracture and small fold structures hosting quartz–gold ore veins was carried out to establish movement along the fault in the ore period. Linear veins with gold–silver–quartz mineralization filling Riedel shear cracks R and R' overprinted

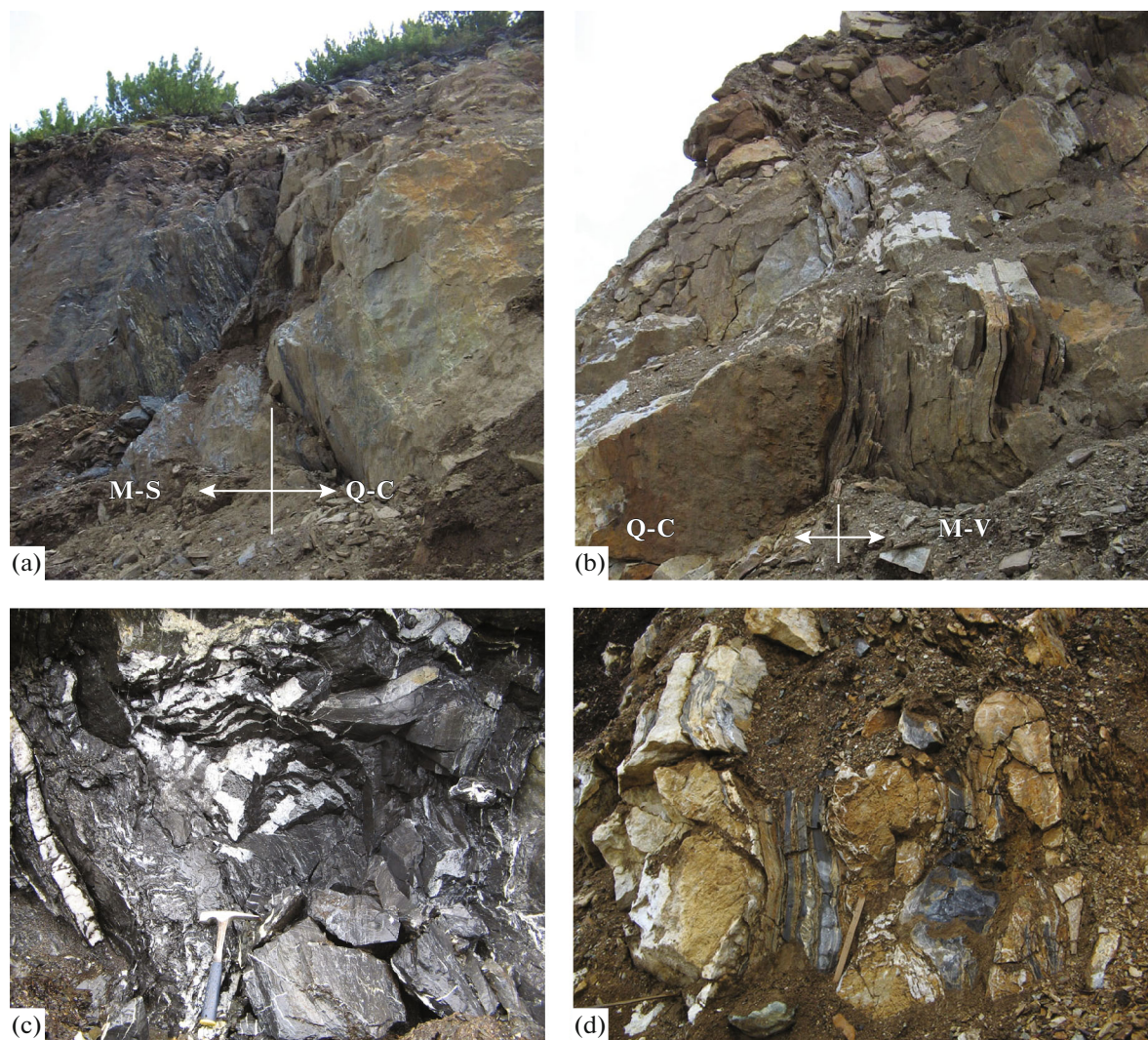


Fig. 2. Contrast tectonites in various segments of Main suture of Syulban fault. (a, b) Segment II (northern part): (a) eastern contact of quartz-carbonate metasomatites (Q-C) with metaschists (M-S) of terrigenous sedimentary sequence; (b) western contact of quartz-carbonate metasomatites (Q-C) with metavolcanites (M-V); (c, d) segment III (central part), (c) metaschist of terrigenous-sedimentary sequence of eastern wall of fault; (d) boudinage in quartz-carbonate metasomatites of fault suture.

on a quartz-carbonate matrix of early metasomatites were observed in three segments of the Syulban fault. These small shear cracks are consistent with the model of (Riedel, 1929) for sinistral shear along the Syulban fault in segment I and dextral shear in segment III. In schists crushed into small isoclinal, overturned folds, mineralization of disseminated gold-silver-sulfide ores and small quartz and sulfide veinlets conformable to the schistosity was observed (Figs. 4a, 4b, 4d). In the eastern exomorphic contact of the Syulban fault, there is a shallow plicature and synore quasi-ductile flow (see Fig. 4c). In the western exomorphic contact of the fault, small drag folds in metavolcanics show no visible signs of ore mineralization conformable to the folding (Fig. 4e). Small near-fault folds in the wall-rocks with axial planes of right or left vergence are confined to a number of sections of the Syulban fault,

which corresponds to the model (Sylvester, 1988) for shear zones. The formation of a quiver-shaped fold (Fig. 5c) in schists can also be attributed to shear paragenesis according to the model (Ez, 2009); however, the crack-seal inclusion band healing of the fold by minerals was formed in elastic seismic deformation conditions that did not cause shear. In addition, veinlets filling conical shear and radial cracks consistent with micro-shear were observed in the schists (Fig. 6c), as well as conical gap fractures (see Figs. 5a, 5b, 5d and Fig. 6b), cross-cutting the schistosity, the formation of which is not explained by any of the mentioned shear models. These brittle failure microstructures filled with mineralization are overprinted on seismogenic dilatation microstructures of the crack-seal inclusion bands.

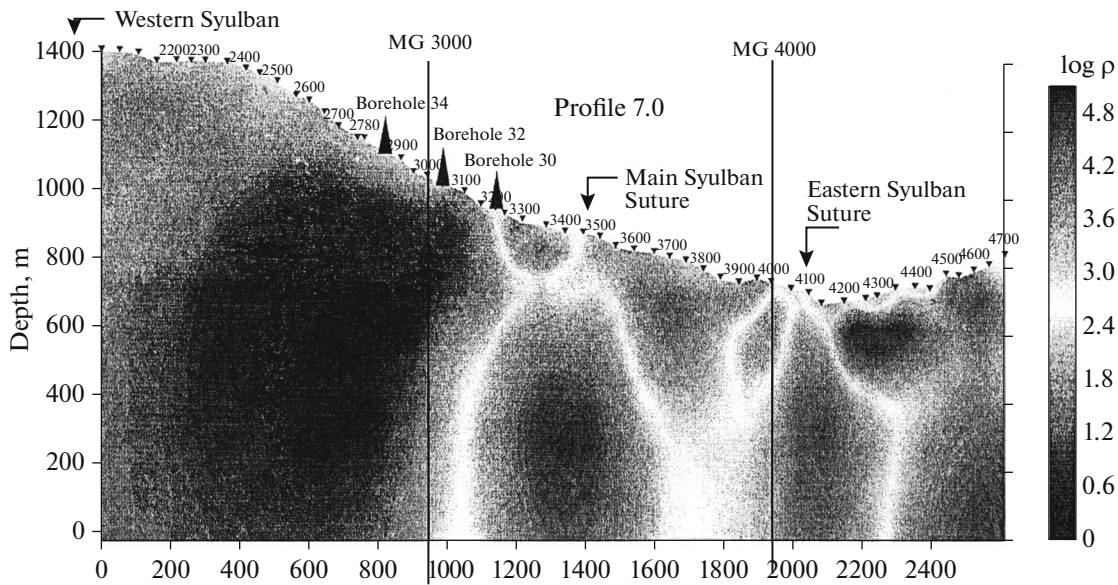


Fig. 3. Geoelectric section according to results of 2D inversion (BIEP method) along profile 7.0 (Danilov et al., 2009f), oriented across Syulban fault system in central part of ore field. Large dispersion between magnetic and induced electromagnetic field (dark, left) are inhomogeneous in magnetic properties of body. Bright, distribution regions of homogeneous quartz–carbonate metasomatites at sutures of Syulban faults.

The contradictory results of the structural–paragenetic analysis suggest that either the type of slip along the faults during fluids injection has not been proved (just like the boundaries of the blocks), or the formation of structural parageneses that do not correspond to the shear models was caused by other mechanisms.

FORMATION OF THE STRUCTURE AND STRUCTURAL PARAGENESES DURING FLUID INPUT

Dynamics of the Change in the SSS of the Medium

Tectonophysical methods established the conical distribution of strain vectors (A, B, C) on the Schmidt grid (see Fig. 7)—the areas of the vectors exiting onto the upper hemisphere are controlled by the projections of the sections of the cones. The revealed variations of the SSS environment: 1) tensile vectors σ_1 (A) are concentrated in the center of the cone, and the intermediate stress vectors σ_2 (B) and compression σ_3 (C) form maximum belts at the boundary of the cone; 2) the compression vectors σ_3 are concentrated in the center of the cone (C), and the vectors σ_1 (A) and σ_2 (B) form the maximum belts along the periphery of the cone. In geological practice, cases are known of conical distribution of vectors reconstructed (Sim, 2017) by the method (Gushchenko, 1979) in rock crystal deposits of the Subpolar Urals. Such a distribution corresponds to either uniaxial tension if only the vectors σ_1 plot in the cone, or uniaxial compression if only vectors σ_3 plot in the cone. The distribution of strain vectors A or C in this case is controlled by the

axis of symmetry of a cone with a circular cross section. In contrast to these data, we obtained a distribution of the strain vectors (A, B, C) bounded by cones with an ellipsoidal cross section, the orientations of the axes of symmetry of which were shifted relative to the axis of cones with a circular cross section. The exact orientations of the axes of symmetry of cones (H) with an ellipsoidal cross section are determined using grids representing isometric projections of a Schmidt grid oriented at different angles to the horizontal plane (small circles of a regular Schmidt grid in an isometric projection are ellipses). Spherograms of the Uryakh strain system reflect both a clear conical distribution of vectors A, B, C (Fig. 7b) and, at first glance, their chaotic distribution (Fig. 7a).

Statistical data processing using the criterion (Bingham, 1974) made it possible to estimate, with varying degrees of probability (60, 70, 80%), the confidence intervals of the conical distribution of vectors A, B, C. They correspond to projections of the sections of the approximating cones on the spherograms (see Fig. 7) As a result, the patterns of the obtained distributions are revealed and the early and late phases of the deformation process are identified. The early phase is characterized by predominant deformations caused by a distribution of vectors A, B, C predominantly around the gently sloping centering axis H of the cone (see Fig. 7a). The late phase corresponds to the distribution of vectors A, B, C around a steeply or obliquely oriented H axis (see Fig. 7b). From a structural point of view, veinlets filling fissures of late deformation systems crosscut veinlets localized in the fissures of early systems.

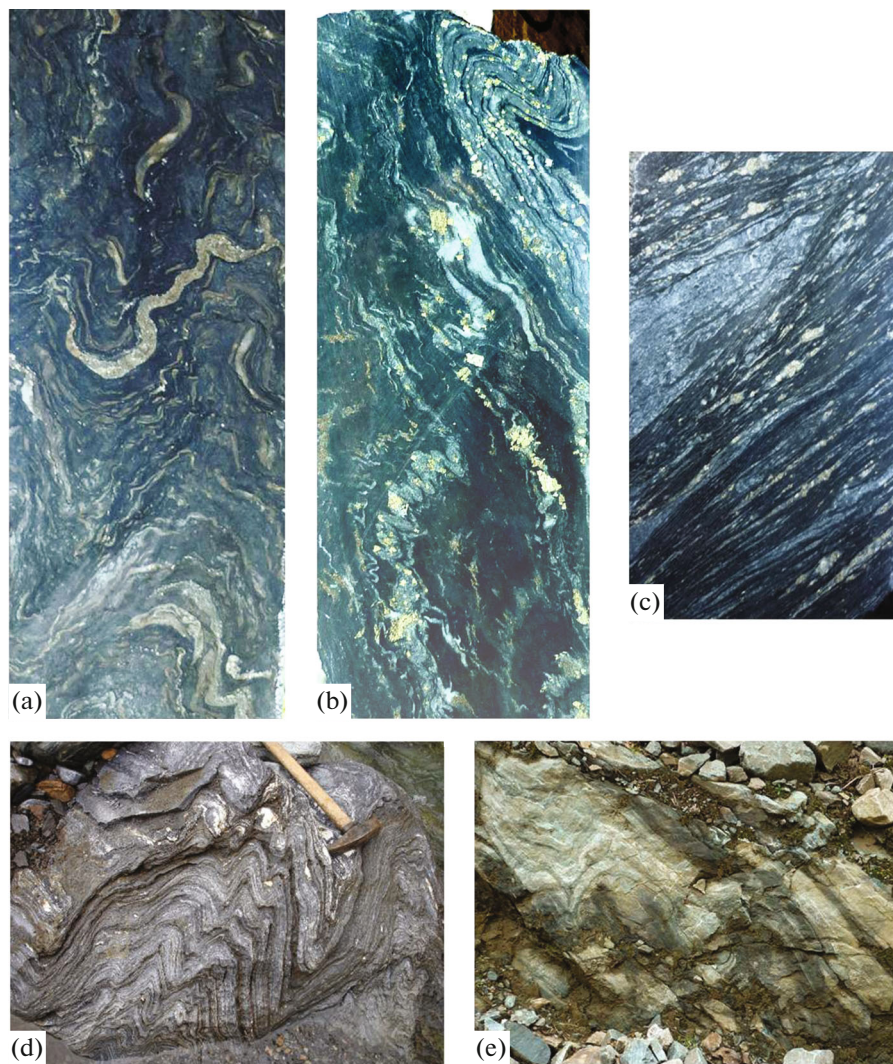


Fig. 4. Small structural forms in zone of influence of Syulban fault. (a, b, c) (photos of polished hand specimens), quasi-ductile syn-ore flow: (a, b) microfolding of schist sequence; (c) boudins in schist not crushed into folds; (d, e) (photos of outcrops) near-fault folds: (d) in schists (Malachite sector), (e) metavolcanites (Vetvisty sector).

Analysis of the local stress fields that caused deformations in the early phase have established unstable dynamic regimes with inversion of vectors σ_1 , σ_2 , σ_3 and with a change in the quantitative estimate of the SSS environment (Table 1). Uniaxial gently sloping (oblique) oriented compression or uniaxial gently sloping (obliquely) oriented tension predominated. Based on generalized samplings, uniaxial compression changed to uniaxial tension during stress redistribution according to the scheme $\sigma_3 \approx \sigma_2 > \sigma_1 \leftrightarrow \sigma_3 \approx \sigma_2 < \sigma_1$, $\sigma_3 \leftrightarrow \sigma_1$. On the whole, a dynamic system developed in an unstable impulsive regime, in which either compressive or tensile stresses are more active. Stresses that caused deformations in the late phase are characterized by a more stable regime of uniaxial sub-vertical extension (see Table 1). This regime caused a more clearly structured deformation with a closed

beltlike distribution of the gently sloping vectors C and B (for $\sigma_3 \approx \sigma_2$) and a polar distribution of vector A near the vertical H axis. For the early phase of variable uniaxial compression/tension we obtained the relation for the Bingham coefficients ($k_1 < k_2 \leq 0$, $k_1 \leq k_2 < 0$), indicating significant asymmetry of the stress tensors with respect to its principal components. The dynamically more stable uniaxial tensile stress field, which caused late-phase deformations, is characterized by tensors with infinitely small asymmetry, which follows from the relation $k_1 \leq k_2 \approx 0$. Given that the asymmetry of the stress tensors is an indicator of the degree of destabilization of the dynamic system during transient seismic conditions, it could only have been triggered in the early phase by injective hydrodynamic stress (fluid pressure). The most stable for this indicator, just like in the stereographic deformation pattern, was the

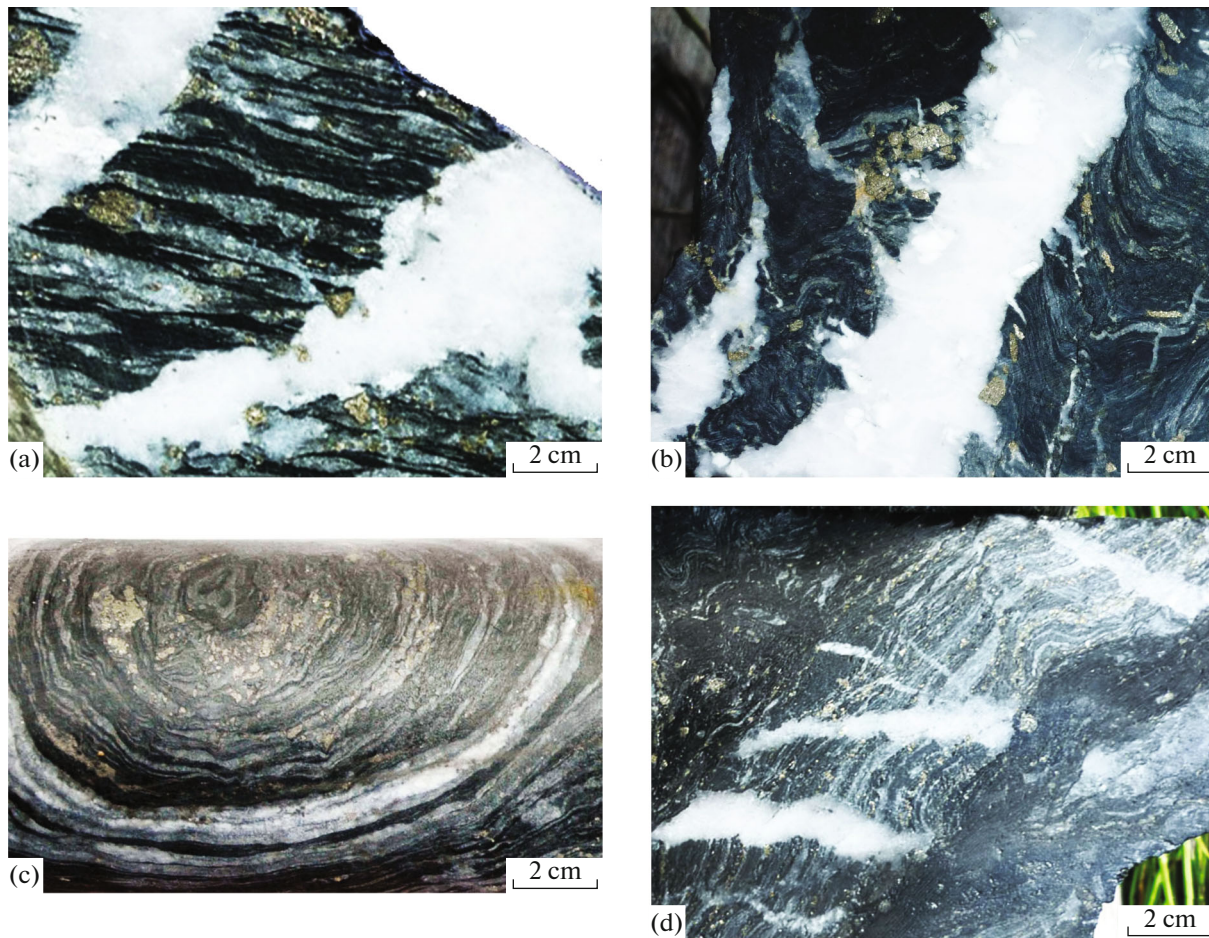


Fig. 5. Structural elements of fracture infrastructure containing Q–Au veins: (a) veins in conical gap fractures in schists (hand samples); (b) combination of conical gap fractures and radial shear cracks superimposed on shallow near-fault folding in schist (polished section of core sample); (c) dilatation microstructures of the crack–seal inclusion bands in crest of small quiver-shaped fold in schist, formed from shear (core sample); (d) combination of vergent conical gap fractures and filamentous radial shear cracks superimposed on dilatation microstructures of the crack–seal inclusion bands in foliated schist sequence (polished sample in area of minor near-fault folding in schist).

development of the SSS environment in the late phase. Such data indicate a change in the uniaxial regime of variable compression/tension to a regime of stable uniaxial tension, as well as the external factor of destabilization of the dynamic system.

For the stable late-phase regime, a geometric stereotype of the distribution of vectors σ_1 , σ_2 , and σ_3 was found among the modern seismodynamic regimes established from the results of stress monitoring of the Kuril Island arc (Zlobin, 1987, Appendix 1); we processed it on a Schmidt isometric grid. This regime is characterized by a sampling (Table 2) of seismic events with hypocenters at a depth of 30 km that occurred sequentially over the course 17 h 28 min in the radius of 147.70–148.00 E and 43.10–43.60 N. Analysis of this sample showed that the strain ellipsoid rotates around the H axis from the previous seismic event to the next. The time between these events is from 10 min

to 7 h 21 minutes. However, it was impossible to establish correspondence between the seismic stereotype and the geometric distribution of the stress–strain vectors of the early phase of the Uryakh dynamic system.

The nature of the SSS environment of the early phase was revealed in all sectors of the ore field (from measurements at ten sites), and the nature of the late-stage SSS environment was also revealed (from measurements at seven sites) only in the Vetvisty and Malakhitovy sectors, and fragmentarily in the Valunny (1 site) and Zolotoi (2 sites) sectors.

Changes in the Fluid Regime in the Stress, Strain, and Temperature Fields

In quartz from samples recovered from ores veins, FI larger than 10 μm in size suitable for microthermometric studies were detected. Based on the phase com-



Fig. 6. Structural elements of fracture infrastructure of Syulban fault zone containing Q–Au veinlets: (a) tangential shear fissures in metavolcanic rocks (outcrop); (b) combination of crack–seal inclusion bands in schists and conical gap fractures, crosscutting schistosity (hand sample); (c) combination of small radial and conical shear fractures, as well as micro–shear (M) superimposed on crack–seal inclusion bands of schist sequence (polished section of core sample from minor near–fault folding zone); (d) combinations of small conical shear fractures forming S-shaped features filled with sigmoid veinlet in plagiogranites (outcrop).

position at room temperature, the primary inclusions were divided into three types: 1, carbon dioxide–water with a gas bubble containing liquid CO₂ (Figs. 8a, 8b); 2, gas filled with dense carbon dioxide (Figs. 8c, 8d); 3, two-phase gas–liquid water–salt solutions (Figs. 8e, 8f).

The results of thermo- and cryometric studies of 139 individual FI are presented in Table 3. The highest homogenization temperatures were obtained for heterogeneous fluids; therefore, correction for the influence of pressure is not required for homogenization

Fig. 7. Spherograms of triads of strain vectors A, B, C of the early (a) and late (b) phases reconstructed from measurements of conjugate veinlets at sites located in ore mineralization occurrence area. Strain (stress) vectors: A (σ_1), tension; B (σ_2), intermediate; C (σ_3), compression; entry of vectors to upper hemisphere of Schmidt grid are shown in distribution density contours, 0.5–1–1.5–2–2.5–3–4.5 ... 7%; triangle, projection of axis of center of cone (H) with ellipsoidal cross section; arcs with dotted lines, projections of approximating Bingham cone cross sections. Numbers of spherogram triads (top left) correspond to numbers of sites in Fig. 1c.

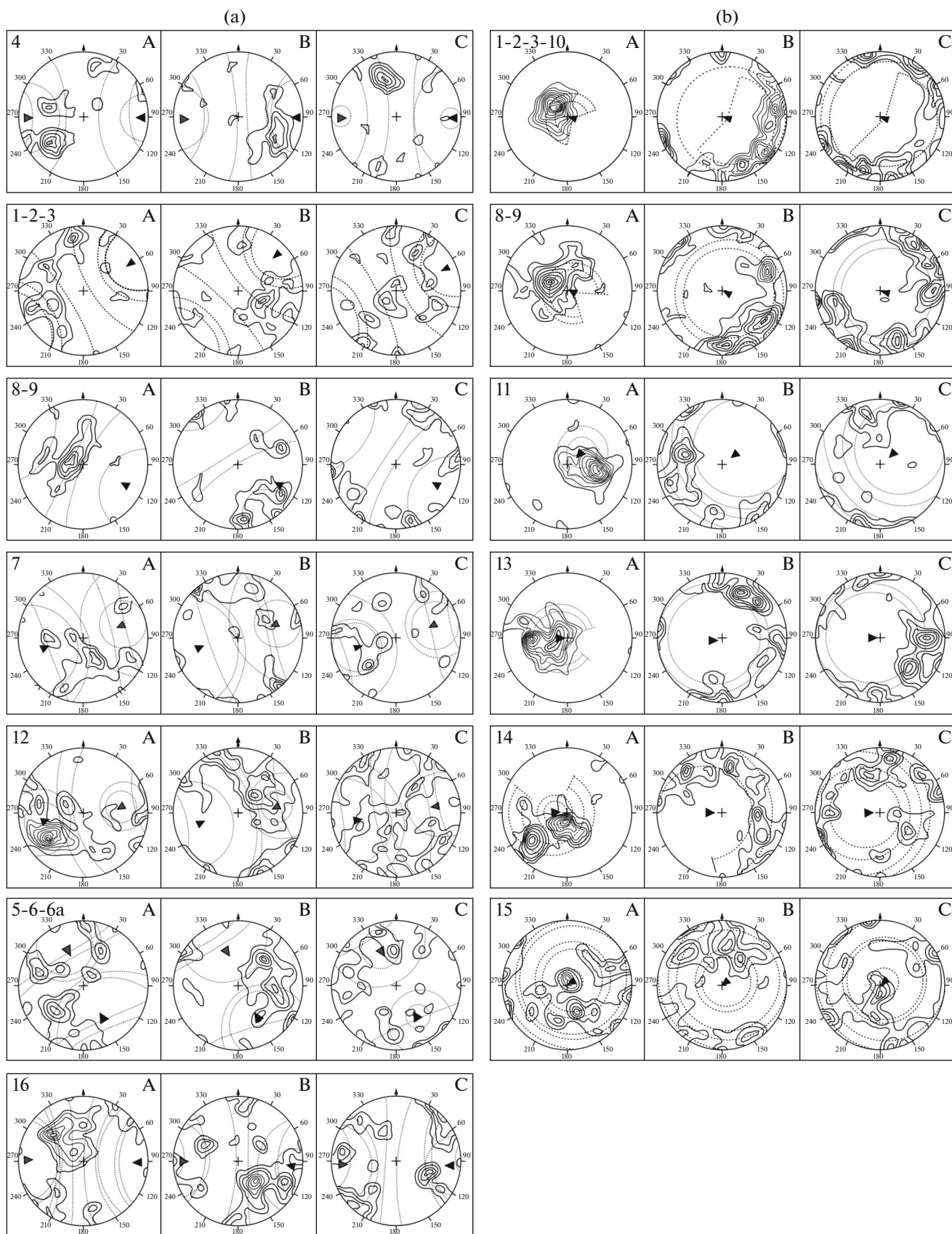


Table 1. Estimates of relative elongation (shortening) of main normal stress vectors in blocks of Uryakh gold ore field

Block number	Early phase of SSS					Late phase of SSS				
	$t_1 (\sigma_1^*)$	$t_2 (\sigma_2^*)$	$t_3 (\sigma_3^*)$		prevailing regime in block	$t_1 (\sigma_1^*)$	$t_2 (\sigma_2^*)$	$t_3 (\sigma_3^*)$		prevailing regime in block
I	0.48	-0.23	-0.21	t	in variable tension \leftrightarrow compression regime ($\sigma_1 > \sigma_2 \approx \sigma_3 \leftrightarrow \sigma_1 < \sigma_2 \approx \sigma_3$) uniaxial tension predominates ($\sigma_1 > \sigma_2 \approx \sigma_3$)	0.43	-0.19	-0.22	t	Uniaxial tension regime $\sigma_1 > \sigma_2 \approx \sigma_3$
	0.57	-0.24	-0.30	t		0.49	-0.21	-0.25	t	
	-0.36	+0.19	0.18	c						
II	-0.48	+0.26	0.23	c	in variable tension \leftrightarrow compression regime ($\sigma_1 > \sigma_2 \approx \sigma_3 \leftrightarrow \sigma_1 < \sigma_2 \approx \sigma_3$) uniaxial compression predominates ($\sigma_1 < \sigma_2 \approx \sigma_3$)	—	—	—		
	-0.56	+0.28	+0.29	c						
	+0.71	-0.37	-0.33	t						
III	0.70	-0.34	-0.35	t	in variable tension \leftrightarrow compression regime ($\sigma_1 > \sigma_2 \approx \sigma_3 \leftrightarrow \sigma_1 < \sigma_2 \approx \sigma_3$) uniaxial tension predominates ($\sigma_1 > \sigma_2 \approx \sigma_3$)	0.76	-0.34	-0.38	t	stable uniaxial tension regime $\sigma_1 \gg \sigma_2 \approx \sigma_3$
	0.68	-0.32	-0.34	t		0.73	-0.32	-0.38	t	
	-0.37	0.17	0.19	c		0.70	-0.35	-0.32	t	
	-0.31	0.14	0.16	c		0.68	-0.28	-0.31	t	
	0.63	-0.29	-0.33	t		0.74	-0.39	-0.31	t	
IV	+0.79	-0.39	-0.38	t	in regime of variable tension \leftrightarrow compression ($\sigma_1 > \sigma_2 \approx \sigma_3 \leftrightarrow \sigma_1 < \sigma_2 \approx \sigma_3$) uniaxial tension predominates ($\sigma_1 > \sigma_2 \approx \sigma_3$)	—	—	—		
	-0.33	0.15	0.19	c						
	0.71	0.31	-0.38	t						

* σ_1 , min compression; σ_2 , intermediate compression; σ_3 , max compression; t, uniaxial tension; c, uniaxial compression.

Table 2. Results of stereogeometric processing of seismic data (selection from data in (Zlobin, 1987, Appendix 1)) for cascade of eight earthquakes that occurred sequentially during 17 h 28 min within a radius of 147.70°–148.00° E and 43.10°–43.60° N

	no. of neighboring events (hypocenter, km)	Angle of rotation of strain ellipsoid around H* left (deg)	Orientations of strain vectors** (dip azimuth/angle, deg)						Magnitude	Time between events (h:min:s)
			T \approx σ_1		B \approx σ_2		P \approx σ_3			
			azimuth	angle	azimuth	angle	azimuth	angle		
1	57(30)	260	2	17	256	42	108	42	5.8	2:4:00
	58(30)		12	13	25	43	230	42	5.2	
2	58(30)	180							5.2	3:40:00
	59(30)		324	2	231	42	55	47	5.6	
3	59(30)	160							5.6	0:15:00
	60(29)		347	4	252	48	80	40	5.1	
4	60(29)	40							5.1	2:13:00
	61(30)		312	12	203	54	47	32	5.3	
5	61(30)	320							5.3	7:21:00
	62(30)		186	0	276	57	90	31	6.8	
6	62(30)	280							6.8	0:10:00
	63(30)		86	0	356	55	175	34	5.7	
7	63(30)	80							5.7	1:45:00
	64(30)		176	3	271	58	85	30	4.7	

* Obtained by stereogeometric constructions; ** obtained from seismic data (Zlobin, 1987). Principal normal strain vectors T, B, P correspond to geological vectors A, B, C.

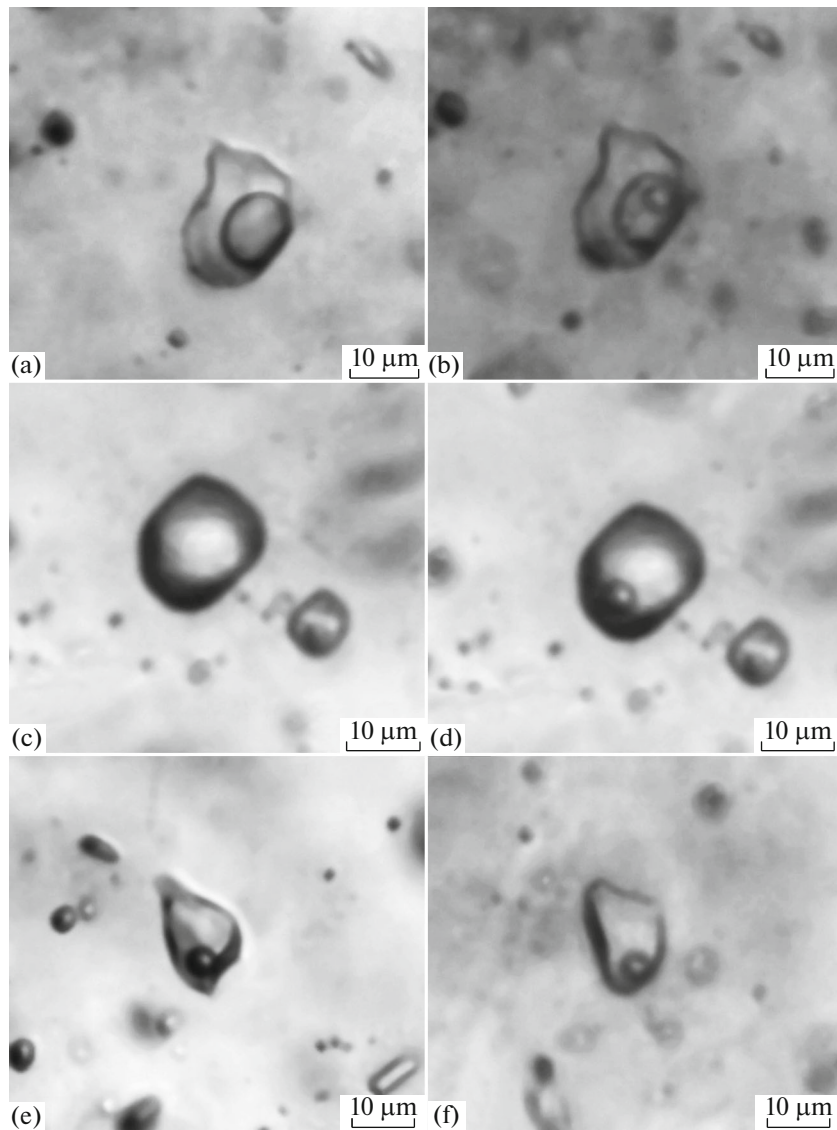


Fig. 8. Fluid inclusions in vein quartz of Uryakh ore field: (a, b) carbon dioxide-water type 1 ((a) +20°C, (b) +8°C); (c, d) gas type 2 ((a) +20°C, (b) -20°C); (d, e) two-phase gas-liquid type 3. Scale 10 µm.

temperatures (Roedder, 1984); they correspond, within the accuracy limits of the method, to the host mineral crystallization temperatures. The homogenization temperatures of primary and primary–secondary FI of the first type vary from 361 to 213°C. The salt concentration in a solution of this type of FI is 5.2–2.5 wt % eq NaCl, and carbon dioxide, 8.5–3.8 mol/kg of solution. The density of carbon dioxide–aqueous fluid is 1.08–0.96 g/cm³. Homogenization of carbon dioxide of the second type of FI occurs in the liquid phase at temperatures from -14.3 to +25.6°C. The melting points of CO₂ changed in them from -57.0 to -59.1°C, which is lower than the melting point of pure CO₂ (-56.6°C) and may indicate an admixture of low-boiling gases (nitrogen, methane). The density of the gas phase is quite high and varies from 0.70 to 1.01 g/cm³. The

large range of carbon dioxide density values in the second type of FI (see Table 3) may be related to the fact that degassing of the Uryakh fluid system occurred under decompression boiling conditions.

The fluid pressure estimated for assemblages of inclusions of the first and second types trapped during periods of a heterogeneous fluid state varies from 3000 to 1120 bar with a change in temperature from 361 to 289°C (see Table 3). When the database is replenished with new results, the limiting *PT* parameters may change slightly. The possibility of reconstructing the formation depth of the deposits based on geological data is in many cases problematic (Safonov, 2000) due to the incompleteness of the geological record. Sample estimates of the depth of mineralization formation of the Uryakh ore field are given in Table 4. Depth Z_L ,

Table 3. Data of thermo- and cryometric studies of individual fluid inclusions in quartz of veins of Uryakh ore field

Sample no.	Type of inclusions*	n	T_{hom} , °C	T_{out} , °C	$T_{\text{melt. ice}}$, °C	$T_{\text{melt. CO}_2}$, °C	$T_{\text{hom. CO}_2}$, °C	$T_{\text{melt. gas hydr}}$, °C	C_{salts} , wt %-eq. NaCl	$C_{\text{CO}_2/\text{CH}_4}$, mol/kg solution	d , g/cm ³	P , bar
C-1	1 P	13	289–293	–30...–34	–4.8...–7.1	–57.3...–58.0	–8.8...+20.1 L	7.3–9.2	2.5–5.2	4.6–7.7/0.6–0.9	0.96–1.06	1120–2820
	2 P	34	–	–	–	–57.3–59.1	–14.3...25.6 L	–	–	–	0.70–1.01	–
C-10	1 P-S	4	213	–30	–6.6	–58.1	–30.9 L	7.3	5.2	3.8/0.3	1.08	–
	3 S	8	191	–30	–5.9	–	–	–	9.1	–	0.94	–
C-5	1 P	6	314–361	–32...–34	–4.8–6.9	–57.3...–57.7	–8.8...–2.0 L	9.1–9.2	2.5–4.5	5.0–8.5/0.6–0.94	1.06	1680–3000
	2 P	53	–	–	–	–57.4...–57.6	–5.6...16.2 L	–	–	–	0.81–0.96	–
C-5	1 P	6	305	–34	–6.8	–57.1	3.6 L	8.0	4.7	7.1/0.9	1.03	1820–2450
	2 P	15	–	–	–	–57.0...–57.1	–3.4...–11.6 L	–	–	–	0.85–0.95	–

* 1, carbon dioxide–water; 2, gas; 3, two-phase gas–liquid. Genetic type of inclusions: P, primary; P-S, primary secondary; S, secondary. n, number of inclusions. L, homogenization of carbon dioxide into liquid phase; G, into gas phase.

Table 4. Estimates of depth of mineralization formation of Uryakh ore field from data on PT parameters of mineral-forming fluids

T_{\max} (°C)	T_{\min} (°C)	T_{\min} corrected for P , min (°C)	P_{\max} (bar)	P_{\min} (bar)	P_{\max}/P_{\min}	Z_L^* (depth, km)	Z_H^{**} (depth, km)	Z_T^{***} (depth, km)	$Z_L - Z_H$ (km)	$Z_L - Z_T$ (km)
361	191	256	3000	1120	2.68	11.54	11.20	8.53	0.34	3.01

Depths calculated: * from lithostatic pressure gradient for values of maximum fluid pressure; ** hydrostatic pressure gradient for minimum fluid pressure; *** from geothermal gradient for minimum temperature taking into account correction for minimum fluid pressure.

calculated for the maximum fluid pressure, with allowance for the lithostatic gradient, is 11.54 km, and the depth Z_H , corresponding to the minimum fluid pressure attributed to the hydrostatic gradient is 11.20 km (see Table 4). When the ratio $P_{\max}/P_{\min} = P_L/P_H = 2.6$ is fulfilled, the calculated depth values Z_L and Z_H should coincide (Prokof'ev and Pek, 2015). However, based on the ratio $P_{\max}/P_{\min} = 2.68$, which slightly exceeds $P_L/P_H = 2.6$, it is possible to assume either the formation of a mineral complex under conditions of upward movement mineral deposition level or a slight excess fluid pressure at a certain depth. In the case of formation of a mineral complex under conditions of upward displacement of the mineral deposition level, the trapping of FI could have occurred in a depth interval $Z_L - Z_H = 0.34$ km. This interval is consistent with estimates of changes in the pressure of mineral-forming fluids, but it does not correspond to the actual ore mineralization interval of 0.8 km. The excess fluid pressure at one depth level was 88 bar, but its value cannot be considered anomalous. At the same time, the value of the mineral deposition depth, calculated from the geothermal gradient for the minimum temperature with allowance for the correction for the minimum fluid pressure, is $Z_T = 8.53$ km. The interval between this depth and that calculated from the lithostatic pressure gradient ($Z_L - Z_T$) can be increased to 3.1 km (see Table 4), and the excess fluid pressure here can reach 800 bar, which is confirmed by the high FI decrepitation activity. Later, new data were obtained (Prokofiev et al., 2019) on the limiting parameters for a fluid pressure of 1050–3290 bar, suggesting that the formation of individual veins occurred in the depth interval 10.5–12.5 km with a fluid overpressure reaching 1.6 kbar. We regard a certain discrepancy in the depth estimates as a disruption of the thermobaric regime of the fluid system during earthquakes which was accompanied by dissipation of seismic energy into the environment and a decrease in the depth of the brittle–ductile boundary. In Transbaikalia, the brittle–ductile boundary drops after the main shock by several kilometers (Petrov, 2010). The brittle deformation mechanisms for strong earthquakes ($M > 5$) with distribution modes of hypocenters at depths of <10, <20, and <30 km were established (Wertlib, 1997) in the area adjacent to the Syulban fault. Multiple earth-

quakes with different hypocentral depths lead to rock failure at different depths and the formation of thick (up to 3 km) fluid-saturated fractured–porous layers in the fault zone, characterized by abnormally low seismic wave velocities. In such layers, attributed by (Nikolaevsky, 1996) to crustal seismic waveguides, the values of the thermobaric fluid parameters are $2 \text{ kb} < P < 5 \text{ kb}$, $200^\circ\text{C} < T < 400^\circ\text{C}$ in the depth range of 10–20 km. These values match the PT parameters obtained by use for carbon dioxide–water–salt inclusions of the first and second types (see Table 3), which makes it possible to suggest the formation of brittle deformations influenced by fluid overpressure.

Pulses of dense pressure fluid in a tectonic framework under overpressure periodically augment seismotectonic stresses with bulk stresses acting from the center of mass of the fluid flow. A signature of periodic manifestations of bulk stresses in the total seismodynamic field is significant asymmetry of the total stress tensors (Nikolaevsky, 2010), which we obtained for the early phase of the Uryakh dynamic system. As a result of fracturing caused by the pulsating SSS environment, evacuated fracture zones filled with fluids under decompression conditions, which led to a periodically depressurized fluid system. Variations in pressure (see Table 3) with a small change in temperature— 75°C (Fig. 9a), as well as variations in the fluid density in an impulsive SSS of the early-phase medium (see Table 1) reflect the fluid system's response to recurring fracturing.

Significant concentrations of CO_2 (Fig. 9b), Cl^- , HCO_3^- , Na and Br were detected in the composition of the fluids with low contents of K, Ca, and Mg. Noteworthy is the sufficiently high Br/Cl ratio (0.0193) in fluids of the Uryakh system, if we take into account the maximum recorded Br/Cl ratio (0.030) (Krainov et al., 2004) in waters of the Dead Sea. A value of 0.0193 can be interpreted as an indicator of fluid evaporation under decompression boiling conditions.

The results of a study (Abramov and Groznova, 2015) of FI in quartz from near-ore *beresites* of the Uryakh ore field showed a phase and salt composition similar to *vein fluids*; however, the pressure calculated by the authors for syngenetic carbon dioxide and water–salt inclusions for the temperature range $305\text{--}385^\circ\text{C}$ is 1029–1406 bar. Obviously, the pulse intro-

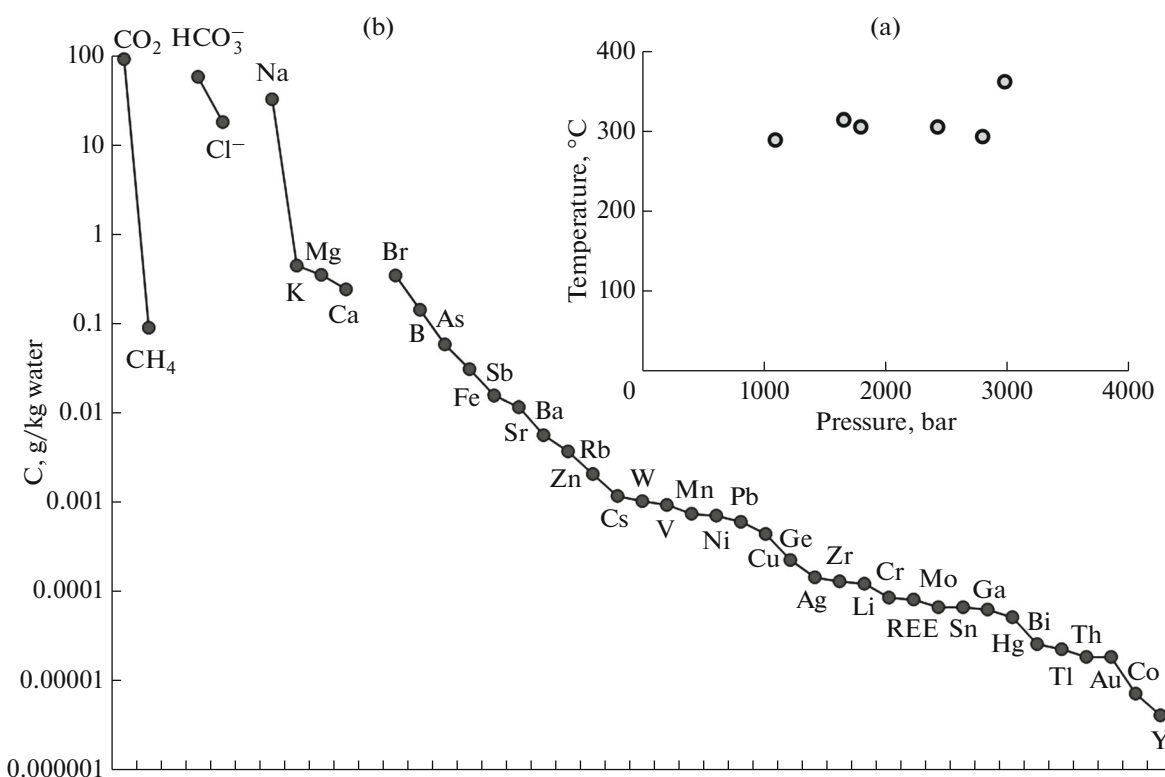


Fig. 9. Plots characterizing *PT*-regime (a) and chemical composition (b) of ore-forming vein fluids of Uryakh ore field.

ducing a large volume of pressure vein fluids under a pressure of 3000 bar into the early phase of seismic activity triggered brittle failure of rocks, resulting in large pressure relief in the fluid system. Beresitization processes occurred after the distribution of the bulk of vein fluids in local fracture spaces at a pressure almost halved.

An FI study of metasomatites by Raman spectroscopy established (Abramov and Groznova, 2015) different N_2 (2.2–21.5 mol %) and CO_2 (76.3–97.9 mol %) ratios, and in one of them, the anisotropic solid phase was identified as nahcolite ($NaHCO_3$). This mineral is unstable in an acidic environment and breaks down when $T = 200^\circ C$. An unstable mineral composition was also obtained by the coauthor of this article based on XRD results for metasomatite samples from borehole 95 located in the Vetyvisty sector in a zone of increased fluid permeability. Water soluble thermonatrite ($Na_2CO_3 \times H_2O$), similar in composition to nahcolite, and amorphous iron and/or manganese oxides are presumably present in one of the samples. Unstable minerals crystallizing in an alkaline medium were found together with minerals crystallizing in acidic conditions in metasomatites formed from protoliths of both metaterrigenous and mafic metavolcanic rocks. The appearance of nachcolite and thermonatrite, unstable in acidic media, may be related to the accumulation of sodium with an increasing role of Mn^{2+}

that replaced iron upon inversion of the fluid regime of the metasomatic process and cyclic degassing of CO_2 . A sharp chemical imbalance may be associated with the reaction of metasomatic fluids to replacement of the early dynamic regime by the late one (metasomatites were recovered in areas where two phases of a change in the SSS of the medium occurred). Such conditions are characterized by accelerated diffusion processes caused by spatiotemporal variations of the filtration properties of the fracture–pore space under the influence of variable compression/tension (Petrov, 2011).

Seismogenic Model of the Formation of Fluid Dynamic Structural Parageneses

To analyze the brittle deformation mechanisms of the Uryakh dynamic system, we used the earthquake mechanism classification developed by (Yunga, 1997), based on geometric typification of the centroid-moment tensors (CMT). The classification scheme determines the permissible areas for seismic mechanisms on a sphere: DC (Double Couple), which result in slip along a single rupture plane (strike-slip, reverse fault, normal fault, etc.), and NDC (Non Double Couple), which form ruptures (fissures) as a result of torsion along several differently oriented planes. The deformation mechanisms were estimated using CMT (Yunga, 1997) from the wave pattern of the seismic

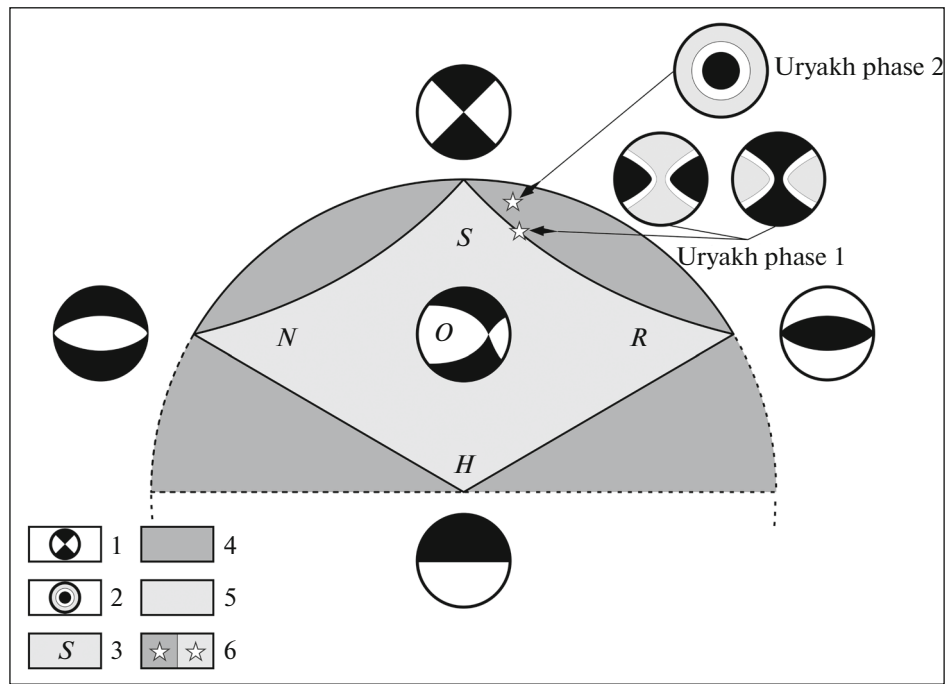


Fig. 10. Classification scheme of seismic deformation mechanisms based on isometric mapping of centroid moment tensors (CMT) onto sphere (after (Yunga, 1997) with additions). (1, 2) diagrams of seismic mechanisms: (1) DC type (black, σ_1 , tensile; white, σ_3 , compression); (2) NDC type (black, σ_1 ; gray, belt distribution σ_2 and σ_3 ; white, deformation shadow); (3) DC types of slip along faults: S, strike-slip fault; R, reverse fault; N, normal fault; H, high-angle fault; O, oblique thrust fault; (4, 5) areas of permissible values into which all CMTs are mapped; (4) forbidden area for DC-mechanisms which noninvertible tensors with $\text{Det}(M_{ij}) = 0$ correspond to; (6) location on diagram of paleomechanisms of Uryakh ore field, which are adequate to seismic ones.

field. We used azimuthal in situ measurements of real brittle paleodeformations, the tensor estimates of the geometric position of which with respect to the basic coordinate system were obtained by the method (Zlobina, 1991), which has a similar classification principle. Tectonic elements of different rank (faults, fissures) and with different orientations having close tensor estimates in the basic coordinate system were attributed to one structural paragenesis formed by one type of local SSS medium.

The results of analyzing the paleomechanisms of brittle deformations of the early phase of the Uryakh dynamic system showed overall their adequacy to the DC seismic mechanism, which caused shear along the fault (Fig. 10). Tensors estimates reflecting shear along the fault and NDC-type fractures fell into the boundary region of permissible values; however, some estimates of the noninvertible tensors corresponding to the forbidden shear region were also depicted here. The brittle paleomechanisms of the late phase have estimates that completely correspond to the region permissible for the CMT (NDC-type fractures), but forbidden to the DC shear mechanism (see Fig. 10). Together with data on the change in varied fluid regime, this means that early-phase brittle deformations formed both as a result of damped shear and fluid pressure, while late-phase brittle deformations were

independent of slip along the fault and were triggered exclusively by pressure fluids.

As a result of the classification, four types of local SSS of the medium are distinguished in the Uryakh ore field in terms of the development of brittle failure in a fluid-saturated medium. The first and second types of SSS of the late phase of seismic activity could have caused fracturing in the medium only under fluid pressure in transensional conditions. The third type of early-phase SSS caused hybrid fracturing under the influence of shear in transensional and fluid pressure conditions. The fourth type of early-phase SSS resulted in hybrid fracturing of the medium also under the influence of shear and fluid pressure, but under transpression conditions. The classification results agree the general regularities of the conical centroid distribution of vectors A, B, C of brittle deformations established by tectonophysical methods: the third and fourth types of SSS correspond to the early phase (see Fig. 7a), and the first and second (see Fig. 7b), to the late phase. Such patterns reflect one geomechanical model of seismogenic fracturing, geometrically represented by tensile (Fig. 11, variants 1–3) and compression cones (Fig. 11, variant 4). The variants of the model (Figs. 11-1, 11-2) reflect fracturing under pressure of upward fluid flow in the late phase, while the other variants (Figs. 11-3, 11-4) characterize the formation of hybrid structural parageneses in the early

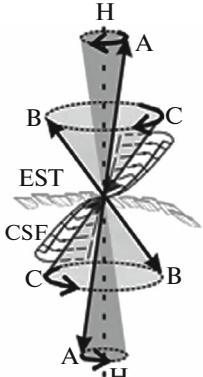
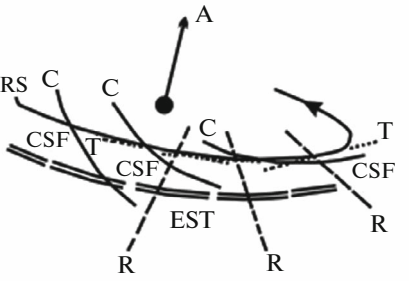
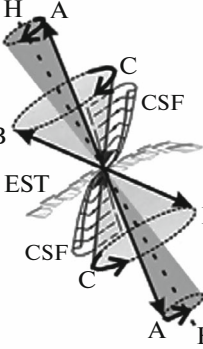
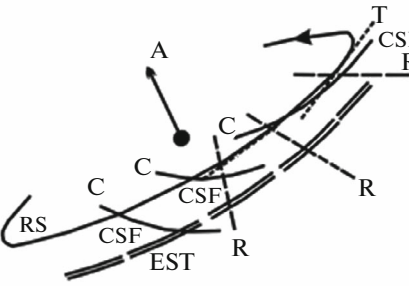
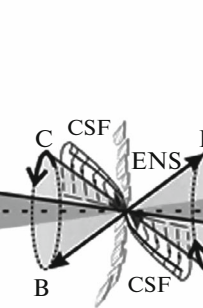
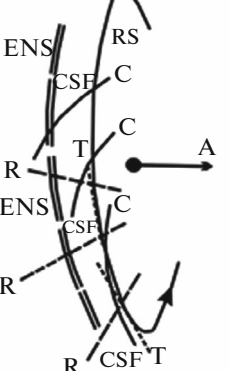
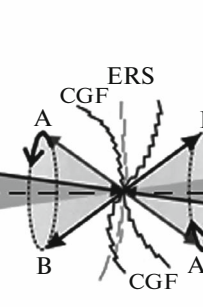
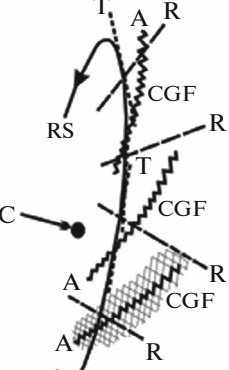
	Variants of deformation model	Kinematic schemes (plan \perp H)	Structural parageneses
1			<p>RS—rotational shear; EST—en echelon gently sloping strike-slip—thrust faults; CSF—conical shear fractures dynamic pair can be propeller-shaped); TT—tangential torsional shear fractures; R—radial gap fractures fractures</p>
2			<p>RS—rotational shear; EST—en echelon gently sloping strike-slip—thrust faults up to 30°–45°; CSF—conical shear fractures dynamic pair can be propeller-shaped); TT—tangential torsional shear fractures; R—radial gap fractures fractures</p>
3			<p>RS—rotational shear; ENS—en echelon normal—strike-slip faults; CSF—conical shear fractures dynamic pair can be propeller-shaped); TT—tangential torsional shear fractures; R—radial gap fractures fractures</p>
4			<p>RS—rotational shear; ERS—en echelon reverse—strike-slip faults CGF—conical gap fractures formed during opening of intersecting gap fractures; TT—tangential torsional shear fractures; R—radial gap fractures fractures</p>

Fig. 11. Variants of deformation model and corresponding kinematic schemes for formation of fractured structural parageneses. Strain vectors: A, tensile; B, intermediate; C, compression. H, strain axis of symmetry. Cones: tension, 1, 2, 3; compression, 4. See text for explanations.

phase. As can be seen from the kinematic schemes corresponding to model variants 1–4 (Fig. 11), the geometry and genotype of the rupture (shear fractures, gap fractures) during the formation of the structural paragenesis depends on the spatial orientation of the axis of the model (H) and on the stress (tension or compression) at the center of the cone. The leading element in the structural paragenesis of fissures is rotational shear formed by the seismic rotation mechanism (NDC type) around the H axis in the plane normal to H. All other elements of the paragenesis—conical shear fractures and gap fractures, radial shear fractures, as well as tangential shear fractures rotating along the surface of the cone, intersect at points on the H axis. The divergence of the conical elements from the H axis depends on the direction of rotation. Geometric modeling of the formation of the fracture structural paragenesis entails coincidence of the H axis of the model with the axis of symmetry of the strain system, the orientation of which is always identical to the channel most fractured and, therefore, permeable to fluids. In this case, the axis of symmetry of the strain system simultaneously controls both the geometry of the elements of progressive failure of the medium and the distribution of fluid flows during fracturing.

The fluid-dynamic structural parageneses that formed in the seismic regime of damped shear, with the participation of the NDC-type seismic torsion mechanism, differ from the standard structural shear paragenesis (Riedel, 1929; Rastsvetaev, 1987; Sylvester, 1988) by the genotype of the formation of rupture elements and the set of linear and nonlinear forms. Some small ruptured and folded forms corresponding to the shear model that arose prior to fluid input have been preserved. Under conditions of elastic seismic deformation, which opened spaces in directions of weakness, dilatation microstructures of the “crack–seal inclusion bands” formed in them.

Features of Block Structure Development and Emplacement of Orebodies in Blocks

In the submeridional ore mineralization zone along the Syulban fault zone, the following spatiotemporal patterns of development of the SSS of the medium have been established, which correspond to variants 1–4 (see Fig. 11) of the fluid-dynamic deformation model. Local dynamic conditions in the process of ore formation differed contrastingly in neighboring segments (I–IV, see Fig. 1c) of the Syulban fault system, separated by transverse faults with sublatitudinal or northeastern strike (Fig. 12).

In segment I, bounded by the Klimovsky and Valunny faults (see Fig. 1c), and in segment III—between the Right Barachny and Yuzhny faults, the early and late phases of development of the SSS environment are established (see Fig. 12-I and 12-III). In the early phase of seismotectonic activity in the regime

of variable compression – tension in these segments, gently sloping stretch prevailed, almost in agreement with the strike of transverse faults. In the late phase, uniaxial tension stretch prevailed in both segments, oriented obliquely in segment I and subvertically in segment III. A sharp change in the orientation of the tensile vectors from gently sloping to subvertical is obviously associated with the compensation of shear stresses on the conducting fault for the input of a large volume of pressure fluids under a pressure of 2–3 kbar in the early phase of seismic activity. This does not contradict the results of analysis of seismic deformation mechanisms, which revealed the decay of shear in the early phase and fracture under pressure of the upward fluid flow in the late phase.

In segment II, located between the Valunny and Pravy Barachny faults, and in segment IV, bounded in the north by the Yuzhny fault, a dynamic medium of variable compression/extension of only the early phase of seismic activity occurred (see Figs. 12-II and 12-IV). However, in segment II, gentle compression predominated in the submeridional direction, consistent with the strike of the Syulban fault, whereas in segment IV, gentle tension in the latitudinal direction prevailed, consistent with the strike of the Yuzhny fault.

Such results prove that during the period of fluid injection, faults transverse to the Syulban system (Klimovsky, Valunny, Pravy Barachny, and Yuzhny) were the boundaries of the tectonic blocks: Klimovsky (I), Valunny–Barachny (II), Stockwork (III), and Yuzhny (IV), which developed in individual local dynamic regimes.

The Valunny–Barachny (II) block, located in the center of the ore field, occupies a special tectonodynamic position. Here, the Syulban fault changes strike in plan view along an arc curved to the west without a change in dip. This block is the only one within the ore field where, under variable compression/tension, compression predominantly parallel to the Syulban master fault prevailed (see Table 1-II) with gently sloping subsidence of vector σ_3 to the south. A low-amplitude sinistral strike-slip has been established along the NE-trending fault bounding the block in the north, and a dextral strike-slip along the latitudinal fault of the southern boundary. The transverse shear–thrust compression duplex system was active here under transpression conditions, while the segment of the Syulban fault developed in this block under conditions that varied from transpression to transtension. For such kinematics of the faults of the two systems, an ore-bearing structural paragenesis formed, which ensured terraced mineralization of orebodies with sublatitudinal and submeridional strike (see Fig. 12-II), not observed in other blocks. Under the influence of a gentle compression, the preore sublatitudinal imbricated thrust fault at the center of the block was reactivated (see Fig. 1c): slip resumed along several fault

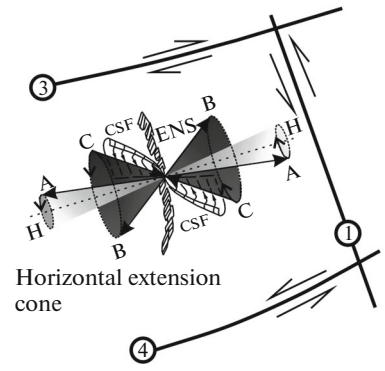
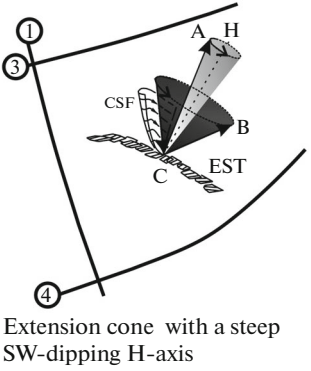
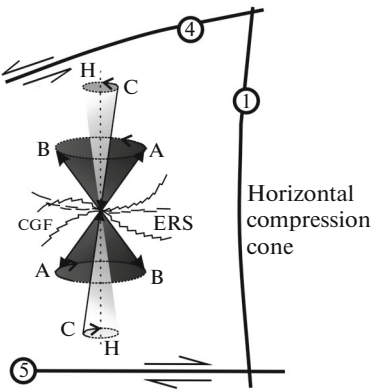
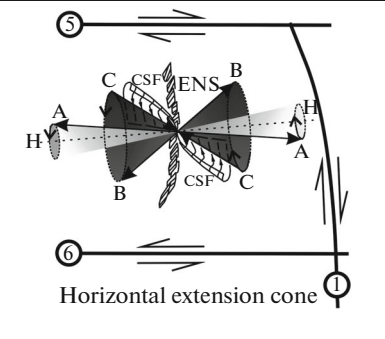
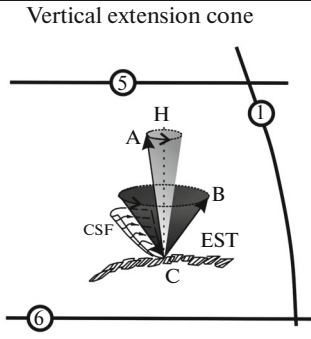
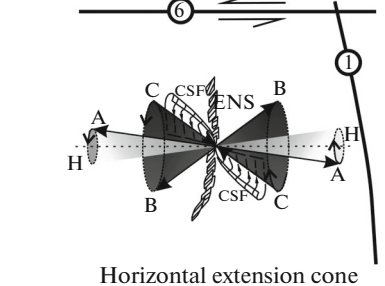
Block	Model variant and its spatial orientation in block with respect to faults		Combined structural–morphological types of orebodies in blocks
	Early SSS	Late SSS	
Klimovsky (I)	 <p>Horizontal extension cone</p>	 <p>Extension cone with a steep SW-dipping H-axis</p>	<p><i>Steeply dipping vein–gangue zones with meridional strike with superposed gently dipping gangue ore mineralization with latitudinal strike, combined with sigmoid veins with meridional and latitudinal orientations; linear stockwork in suture of Syulban fault</i></p>
Valuno-Barachny (II)	 <p>Horizontal compression cone</p>		<p>Tiered mineralization of vein zones, rimmed by stringer-disseminated mineralization with <i>submeridional</i> strike and individual gently sloping veins with <i>sublatitudinal</i> strike</p>
Stockwork (III)	 <p>Horizontal extension cone</p>	 <p>Vertical extension cone</p>	<p>Stockwork mineralization of orebodies: <i>gently sloping</i> stringer-disseminated in beresitization zones and veins in metavolcanic rocks combined with <i>steeply dipping</i> veins with submeridional strike and sigmoid veins; linear stockwork in suture of Syulban fault.</p>
Yuzhny (IV)	 <p>Horizontal extension cone</p>		<p>Combined vein bodies and thin-stringer linear zones with submeridional strike and stringers with sigmoid morphology</p>

Fig. 12. Spatial orientation schemes of strain model variants, which ensured combination of morphological types of orebodies formed in different strain phases in blocks. For numbers of faults in circles and numbers in blocks, see Fig. 11. See text for explanations.

planes normally oriented to the axes of centroid compression. When fluids arrived, the kinematics along the fault planes separating the thrust sheets changed to shear–thrust. In the area of local stress unloading, e.g., sublatitudinal veins formed (no. 8 in schist and no. 8a in metavolcanic rocks) plunging NNW at angles of 35°–45°. Upsection are two large vein zones with submeridional strike: no. 12 in schist, consisting of three large veins, rimmed with veins and disseminated ores; no. 9, including two large veins and near-ore beresites in metavolcanic rocks. The veins of these zones contain radial shear fractures that opened in the schist under the influence of fluids along the foliation, and in the metavolcanics they rejuvenated the kinematics of early simple cleavage fractures. According to the model (see Fig. 12-II), radial shear fractures should have a submeridional orientation, but a variable dip, which corresponds to a different dipping of veinlets. In this block, small conical gap fractures made by ore veins were also noted, the hybrid tectonogenesis of which was most clearly manifested in schist (see Figs. 5a, 5b, 5d).

Yuzhny (IV) block. In the region of the sublatitudinal Yuzhny fault, the change of centroid compression to centroid tension was clearly manifested with the gentle sloping orientation of vectors $\sigma_1 \leftrightarrow \sigma_3$ in the direction to the strike of the fault, at a small angle. This means that in the early phase of seismic activity, the transpression conditions here changed to transtension, which may be associated either with the influence of fluids and/or change in the direction of shear along this fault. Nevertheless, centroid sublatitudinal extension stress predominated in this block (see Table 1-IV, Fig. 12-IV), and we were inclined toward an assessment of sinistral shear, which decays under the influence of fluids. For a sublatitudinal gently sloping H axis, submeridionally trending en echelon normal–strike-slip faults formed (see Fig. 11-3), in which vein nos. 53, 54, 55, 57, 58 were mineralized. Near the Yuzhny fault, veinlets of complex morphology are localized in schist, which were simultaneously filled with small conical and radial shear fractures, as well as dilatation microstructures of the “crack–seal inclusion bands” in the schist, crushed into small fracture folds (see Fig. 6c) and veinlets in plagiogranites with sigmoid morphology (see Fig. 6d). The southern boundary of the block within the area licensed by the Nord-Gold N.V. company was not established.

In the Klimovsky (I) block, the Syulban fault changes dip from west to east due to listric bending in the fault plane. The immersion of the Main Suture of the Syulban fault to depth under the shale sequence obviously had no such effect on the redistribution of stresses as did the activity of transverse faults in the early phase of seismic activity. Sublatitudinal orientations of gently sloping vectors $\sigma_1 \leftrightarrow \sigma_3$ of variable compression/extension of the early phase (see Table 1-I) indicate a change in sinistral shear to dextral along the NE-striking fault planes bounding the block. Revers-

ible low-amplitude slip is one of the reasons for the development of numerous latitudinally striking intra-block fractures (see Fig. 1c), which created a zone of increased permeability here. In this zone, in the late phase of SSS development, obliquely oriented tension prevailed with a steep slope of vector σ_1 to the southwest (Fig. 12-I). Metavolcanic rocks host only a few en echelon veins of zone no. 4, with a meridional strike, schists host the main large vein zones. Near the Main Suture of the Syulban fault there is vein–stringer zone no. 2 with meridional strike, a thickness of 3.5 to 20 m, and a length of more than 1 km, consisting of two large veins steeply dipping to the west. The veins are accompanied by near-ore beresitization of rocks, consistent with quartz veinlets and dilatation microstructures of the crack–seal inclusion bands, overprinted by shallow veins, crosscutting both vein bodies and schistosity (see Figs. 6a, 6b). Exhumed by river erosion 350 m below vein zone no. 2 is the Selevaya vein, with a length of 3360 m, a thickness of 1.5 to 17.5 m, a northwestern strike, steep (80°) dip, and sigmoid morphology. Vein no. 3 also has sigmoid morphology, but a sublatitudinal strike and a much smaller extent. The northwestern linear vein bodies formed in en echelon normal–strike-slip faults in the early phase of seismic activity. Nonlinear small veins and veinlets with sigmoid morphology formed under the influence of fluids in the late phase of seismic activity in conical cleavage fractures under transtension conditions.

In the *Stockwork (III) block,* the Syulban fault has a NNW strike and a steep dip to the southwest and northeast. The opposite dip of the fault is due to the listric S-shaped bend of the vertical plane at the center of the block, which here shaped the fault plane in the form of a propeller. Throughout the development of the Syulban fault, listric wedging influenced the local stress redistribution and rock destruction, which was more intense than in other blocks (see Figs. 2c, 2d). Here, in metavolcanic rocks, three crush zones intersect, paragenetically related to activation of the Syulban fault in different periods, forming a high-permeability region (see Fig. 1c), for which U, Th, and K anomalies were established (Danilov et al., 2009f). Two thick linear zones of tabular crushing of rocks—subvertical and gently sloping—have propagated along to the strike of the Main Suture of the Syulban fault. The third thin tabular subvertical crush zone, with a thickness of up to 10 m, has a sublatitudinal strike and is adjacent to the fault suture in the wedged area at an angle of 45°–50°. During the preore period, the first subvertical crush zone controlled the granitoid distribution (PR₂₋₃) which outcropped on the surface in the form of linear planar bodies, and in ore formation periods, linear zones of beresitization and vein bodies. Here, in a strip up to 800 m wide and 3 km long adjacent to the Syulban fault from the west, boreholes uncovered 30 gently sloping linear zones of beresites with vein–disseminated mineralization. The length of individual ore zones is 0.2–1.5 km, the thickness var-

ies from 5–30 to 80 m, and the dip angles of these zones are 10°–15° east (Vetvisty sector) and west (Malakhitovy sector). The ore zones, represented by flattened bodies of vein-disseminated ores and a system of shallow quartz veins, arranged en echelon both in dip and strike, have a stockwork structure. Gently sloping lenticular veins of small thickness, consistent with the Syulban strike fault, were also discovered on the western flank of the Stockwork block in metavolcanic rocks. In addition, in this block, lenticular veins of similar strike are widespread in schists and metavolcanic rocks, but have a steep dip. In the southern part of the block, riverine erosion has revealed two veins of sigmoid morphology with NW and sublatitudinal strike in faults. During the *early phase*, seismic activity in the Stockwork block was dominated by tensile stresses (see Table 1-III), which caused hybrid deformations according to the variant of the model (see Fig. 11-3). The H axis of the model during this period is oriented normally to the plane of the Main fault plane of the Syulban fault (see Fig. 12-III), so the en echelon normal–strike-slip faults that host steeply dipping veins have a strike consistent with the Main Suture. The orientation of tension changed under the influence of fluids in the *late phase* of seismic activity to subvertical, which led to the formation of gently sloping en echelon strike-slip faults normally oriented toward the H axis and containing small lenticular veins. The gently dipping stockwork ore-bodies in berisites formed under transtension and seismogenic dilatancy conditions. Subsidence of the H axis at an angle of 80° to the west in the Vetvisty sector and to the east in the Malakhitovy sector explains the different dips of gently sloping orebodies at an angle of 10° east and west, respectively. Sigmoid veins and veinlets contain conical shear fractures that formed in the late phase of seismic activity under the influence of fluids under transtension conditions.

The formation of large veins with sigmoid morphology in faults of the *Klimovsky and Stockwork* blocks was probably related to the inherited tectonic voids that formed in faults during shear in the early phase, which is worthy of discussion.

Seismogenic structural paragenesis, which formed with the participation of fluids according to the same conical strain model, formed various combinations of structural–morphological types of ore-bodies in blocks (see Fig. 12).

DISCUSSION

Problems concerning the conical model of synore deformations of the Uryakh gold ore field and its conformability to various DC and NDC earthquake mechanisms are obviously related. Geometric models in the form of tension and compression cones, as well as the idealized diagram of paragenetic families corresponding to these models, have been shown (Rastsvetaev, 1987) in the fields of shear, compressional, and

tensile stresses. In the case of a biaxial shear stress field, many different fracture systems arise (shear, shear–overthrust, normal fault, pull-apart cracks), essentially “rotating” around the axis of symmetry of the strain system and/or normally oriented to it. The axis of symmetry of the strain system coincides with either vector σ_3 in the compression cone or vector σ_1 in the tension cone with a circular section. In these models, there is no mention of the case of equalization with the absolute value $|\sigma_2| = |\sigma_3|$ when a uniaxial conical tensile field arises with the symmetry axis of strain, coinciding with σ_1 , around which the tangential shear fractures that formed at points tangent with a virtual conical surface revolve. Structural parageneses (Rastsvetaev, 1987) do not completely coincide with ours, since the author’s strain models did not take into account the destabilizing effect of pressure of the active fluid flow on the stress field, which leads to distortion of the SSS of the medium and violation of symmetry of the strain system. Under the influence of fluid pressure, the axis of symmetry of the strain system shifts relative to σ_1 , or σ_3 , and the maxima of the other two vectors (σ_2 , σ_3 or σ_2 , σ_1) form belts on the Schmidt grid corresponding to an elliptical cross section of the cone. In the practice of constructing stereogeometric images from in situ data, no method was known for finding the axis of symmetry of a strain system unstable under the influence of fluids. The idea “on using isometric projections of a Schmidt grid to analyze seismic strain systems,” first stated by E.P. Malinovsky (1992, oral communication), was used by us to construct isometric overlays, making it possible to stereogeometrically find the orientation of the axis of symmetry of unstable strain systems.

For seismic mechanisms of NDC-type deformations, it is important to note that they were previously discovered only in the sources of deep-focus earthquakes with hypocenters in the Benioff zone or in the mantle. The reason for their occurrence was explained by (Randall, 1971) as phase transformations of the mantle substance. Later, NDC mechanisms were revealed (Lutikov et al., 2010) in the crust along DC-type mechanisms in the realization of earthquake events in the general regime of uniaxial variable compression/tension. Such data are similar to ours, obtained for the early phase of the SSS medium. The question arises: what was reflected in the “hybrid” early phase of the Uryakh dynamic system—quick replacement of the crustal DC mechanism by a deep-focus NDC mechanism, the reason for which is still a matter of debate, or is the crustal NDC mechanism a product of the phase transition of the shear stress field in the centroid under the influence of fluids?

In the Uryakh gold ore field, the two phases of development of the SSS environment are probably not separated by a large period of seismotectonic quiescence. Discrete–continuous development of seismic centroid events can be judged from the results of dis-

Discussing factual data. When interpreting the time of formation of a set of small structural parageneses, which often overprint dilatation microstructures crack–seal inclusion bands in schists, one gets the impression the microstructures crack–seal inclusion bands form in the early phase and small structural parageneses are superimposed in the late phase of seismic activity. However, crack–seal inclusion bands of the same type during ore formation by a quartz–carbonate material similar in mineral performance form in a setting of elastic deformations both during the early (block I) and late (block III) phases. The actual manifestation of the late phase of the SSS only in these blocks means that the formation of similar crack–seal inclusion bands should occur in the case of a short time between early and late phases of the SSS. The dilatant opening of space in directions of weakness in rock strength occurs always easier and faster than the formation of new fissures under brittle failure conditions when the rock yield strength is achieved; for this reason, brittle deformations are always superimposed on the elastic ones.

The results of studying (Cox, 2016) crack–seal inclusion bands revealed the recurrence intervals of seismic “multiplets” characterizing earthquake swarm events of the same form. The late phase deformation mechanisms of the Uryakh system, similar to the unloading mechanisms of NDC-type earthquake sources, are also uniform in their distinct deformation patterns. Assuming that cascades of aftershocks of such earthquakes with magnitudes 4.7–6.8 (see Table 2) could form a kind of group of multiplets, then it is possible to adopt the following scenario for the formation of large sigmoid veins in faults. Such cascades resulted in pulses of fluids into tectonic voids formed between curved fault walls as a result of shear in the early phase. As a large volume of fluid accumulated in the half-closed voids, the pressure of the fluid system increased, which compensated shear stresses. After shear ceased, the fluids were “locked” in the structural traps of the faults, where veins formed in the late phase. This does not contradict the unified geomechanical model of the formation of hybrid structural parageneses in the early phase of seismic activity and under the influence of fluid overpressure in the late phase.

We are inclined to the version that the NDC mechanism of the Uryakh dynamic system is the product of the phase transition of the shear stress field to centroid under the influence of fluids (Zlobina et al., 2016). The processes of the phase transition of the stress field start at the critical fluid pressure (~3 kbar) and are completed in the case of intensive degassing of the fluid system and boiling of solutions, leading to an increase in salt concentration in them and thermochemical inversion of the fluid composition (Zlobina et al., 2017). The maximum *PT* parameters of the Uryakh fluid–dynamic system were extremely critical, but sufficient for the onset of the process; however, with insufficient fluid degassing, the phase transition

could have been completed only in two nonadjacent blocks (the Klimovsky and Stockwork).

CONCLUSIONS

The formation of gold ore mineralization at the Uryakh ore field occurred in a seismic shear regime along deep fluid-supply faults of the Syulban system and the fault system transverse to it. Tectonophysical methods confirmed the block structure of the ore field and established the individual development of blocks. Overpressure of the fluid flow exerted a destabilizing effect on the seismic stress field, which led to compensation of shear, distortion of the SSS of the medium, violation of symmetry of the strain system, and the formation of structural parageneses differing from shear parageneses. Hybrid structural parageneses form under the influence of decaying shear stresses and injective hydrodynamic stress in an unstable regime of variable compression/extension of the early phase of seismic activity in all blocks. The formation of structural parageneses in the regime of stable uniaxial extension of the late phase of seismic activity occurred in the absence of slip along faults in only two blocks under the influence of fluid overpressure. It is assumed that such a complex symbiosis of brittle deformations formed because the hydrothermal system initiated the phase transition of the seismic field of shear stresses to centroid, which was completed fully only in two nonadjacent blocks.

ACKNOWLEDGMENTS

The authors thank corresponding member of the RAS Yu.G. Safonov for consultations on the ore formation processes in the Uryakh gold ore field, as well as professor of Tomsk Polytechnic University I.V. Kucherenko for useful recommendations on “relating model elements to the real structural framework of the ore field.”

FUNDING

This study was carried out as part of research topic no. in IS GZ 0136-2018-0023, with financial support from the International Nord-Gold N.V. company (research contract nos. D/SSR-11/0313, D/SSR-12/0177, D/SSR-12/0088).

CONFLICT OF INTEREST

The authors declare that they have no conflict of interest.

REFERENCES

Abramov, S.C. and Groznova, E.O., Zoning of metasomatically altered rocks in the Syul’ban gold-bearing zone (Uryakh deposits, Irkutsk obl.), *Petrografiya magmaticheskikh i metamorficheskikh gornykh porod: Mater. KhKhII Vseros. petrografich. Soveshchaniya* (Petrography of Magmatic and Metamorphic Rocks. Proc. 22nd All-Russian Pe-

- trographic Conference), Petrozavodsk: KNTs RAN, 2015, pp. 281–283.
- Angelier, J., Sur l'analyse de mesures recueillies dans des sites failles: l'utilite d'une confrontation entre les methods dynamiques et cinematiques, *Buill. Soc. Geol. France*, 1975, vol. 281, pp. 1805–1808.
- Bingham, Ch., An antipodally symmetric distribution on the sphere, *Ann. Statist.*, 1974, vol. 2, pp. 1201–1225.
- Bingham, Ch. and Mardia, K.V., A small circle distribution on the sphere, *Biometrika*, 1978, vol. 65, pp. 379–389.
- Bodnar, R.J. and Vityk, M.O., Interpretation of microthermometric data for H₂O–NaCl fluid inclusions, *Fluid Inclusions in Minerals: Methods and Applications*, Benedetto De Vivo & Maria Luce Frezzotti, Eds., Pontignano: Siena, 1994, pp. 117–130.
- Borisenko, A.S., Cryometric study of salt composition of gas–liquid inclusions in minerals, *Geol. Geofiz.*, 1977, no. 8, pp. 16–27.
- Bortnikov, N.S., Geochemistry and origin of the ore-forming fluids in hydrothermal–magmatic systems in tectonically active zones, *Geol. Ore Deposits*, 2006, vol. 48, no. 1, pp. 1–22.
- Bortnikov, N.S., Prokof'ev, V.Yu., and Razdolina, N.V., Origin of the Charmitan gold–quartz deposit (Uzbekistan), *Geol. Ore Deposits*, 1996, vol. 38, no. 3, pp. 238–257.
- Bortnikov, N.S., Gamyarin, G.N., Alpatov, V.A., Naumov, V. B., Nosik, L.P., and Mironova, O.F., Mineralogy, geochemistry and origin of the Nezhdaninsk gold deposit (Sakha-Yakutia, Russia), *Geol. Ore Deposits*, 1998, vol. 40, no. 2, pp. 121–138.
- Bortnikov, N.S., Murzin, V.V., Sazonov, V.N., Prokof'ev, V.Y., and Stolyarov, M.I., The Svetlinsk gold–telluride deposit, Urals, Russia: mineral paragenesis, fluid inclusion and stable isotope studies, *Mineral Deposits: Processes to processing*, London, 1999, pp. 21–24.
<https://doi.org/10.13140/2.1.3358.2727>
- Bortnikov, N.S., Bryzgalov, I.A., Krivitskaya, N.N., Prokof'ev, V. Yu., and Vikent'eva, O.V., The Maiskoe multimegastage disseminated gold–sulfide deposit (Chukotka, Russia): mineralogy, fluid inclusions, stable isotopes (O and S), history, and conditions of formation, *Geol. Ore Deposits*, 2004, vol. 46, no. 6, pp. 409–440.
- Brown, P., FLINCOR: a computer program for the reduction and investigation of fluid inclusion data, *Am. Mineral.*, 1989, vol. 74, pp. 1390–1393.
- Chugaev, A.V., Nosova, A.A., Abramov, S.S., Chernyshev, I.V., Bortnikov, N.S., Larionova, Yu.O., Gol'tsman, Yu.V., Moralev, G.V., and Vol'fson, A.A., Early Permian stage of formation of gold-ore deposits of Northeastern Transbaikalia: isotope-geochronological (Rb–Sr and ³⁹Ar–⁴⁰Ar) data for the Uryakh Ore Field, *Dokl. Earth Sci.*, 2015, vol. 463, no. 6, pp. 700–704.
<https://doi.org/10.7868/S0869565215240172>
- Connolly, J.A.D. and Petrini, K., An automated strategy for calculation of phase diagram sections and retrieval of rock properties as a function of physical conditions, *J. Metamorph. Petrol.*, 2002, no. 20, pp. 697–708.
<https://doi.org/10.1046/j.1525-1314.2002.00398.x>
- Cox, S.F., Faulting processes at high fluid pressures an example of fault-valve behavior from the Wattle Gutly Fault, Victoria, Australia, *J. Geophys. Res.*, 1995, no. 100, pp. 12841–12859.
<https://doi.org/10.1029/95JB00915>
- Cox, S.F., Coupling between deformation, fluid pressure and fluid flow in ore-producing hydrothermal systems at depth in the crust, *Econ. Geol.*, 2005, vol. 100, pp. 39–75.
- Cox, S.F., Injection-driven swarm seismicity and permeability enhancement: implication for the dynamics of hydrothermal ore systems in high fluid-flux, overpressured faulting regimes, *Econ. Geol.*, 2016, vol. 111, no. 3, pp. 559–587.
<https://doi.org/10.1016/j.econgeol.2016.04.001>
- Ez, V.V., *Nauchnye trudy* (Transactions), Moscow: IFZ RAN, 2009. 234 s.
- Gushchenko, O.I., *Method of kinematic analysis of destruction structures in reconstructing tectonic stress fields, Polyapryazhenii i deformatsii v litosfere (Stress and Deformation Fields in the Lithosphere)*, Moscow: Nauka, 1979, pp. 7–25.
- Gzovskii, M. V., *Osnovy tektonofiziki* (Principles of Tectonophysics), Moscow: Nauka, 1975.
- Karasev, P.S., Seismotectonics of the Transition Area from the Baikal Rift Zone to the Rise of Stanovoy Range, *Extended Abstract of Candidate's (Geol.-Min) Dissertation*, Moscow: MGU, 2009.
- Krainov, S.R., Ryzhenko, B.N., and Shvets, V.M., *Geokhimiya prirodnykh vod. Teoreticheskie, prikladnye i ekologicheskie aspekty* (Geochemistry of Natural Waters. Theoretical, Applied, and Ecological Aspects), Moscow: Nauka, 2004.
- Kryazhev, S.G., Prokof'ev, V.Yu., and Vasyuta, Yu.V., Application of ICP-MS in analyzing ore-forming fluids, *Vestn. Mosk. Gos. Univ., Ser. 4, Geol.*, 2006, no. 4, pp. 30–36.
- Kucherenko, I.V. and Gavrilov, R.Yu., Structural-dynamic modes of the formation of the gold–sulfide–quartz mineralization in the Syul'ban gold-bearing zone (Vitim River middle reaches basin). Part. 1. Karalon ore field, *Izv. Tomsk. Politekh. Univ.*, 2011, vol. 318, no. 1, pp. 29–35.
- Kucherenko, I.V. and Gavrilov, R.Yu., Structural-dynamic modes of the formation of the gold–sulfide–quartz mineralization in the Syul'ban gold-bearing zone (Vitim River middle reaches basin). Part. 2. Uryakh ore field, *Izv. Tomsk. Politekh. Univ.*, 2012, vol. 320, no. 1, pp. 19–27.
- Lutikov, A.I., Yunga, S.L., and Kuchai, M.S., Seismic sources unsatisfying the double dipole model: criteria for revealing and distribution in island arcs, *Geofiz. Issled.*, 2010, vol. 11, no. 3, pp. 11–25.
- Mitrofanov, G.L., Tectonic Principles of Localization and Formation of Noble Metal Deposits in the Southern Framing of the Siberian Platform, *Extended Abstract of Doctoral (Geol.-Min) Dissertation*, Moscow: IGEM RAN, 2006.
- Nguyen, P.T., Cox, S.F., Harris, L.B., and Powell, C.A., Fault-valve behavior in optimally oriented shear zones: an example at the Revenge gold mine, Kambalda, Western Australia, *J. Struct. Geol.*, 1998, vol. 20, no. 12, pp. 1625–1640.
[https://doi.org/10.1016/S0191-8141\(98\)00054-6](https://doi.org/10.1016/S0191-8141(98)00054-6)
- Nikolaevskii, V.N., *Geomekhanika i flyuidodinamika* (Geomechanics and Fluid Dynamics), Moscow: Nedra, 1996.
- Nikolaevskii, V.N., *Geomekhanika. Sobranie trudov, vol. 2. Zemnaya kora. Nelineinaya seismika. Vikhri i uragany* (Geomechanics. Transactions. Volume 2. Earth's Crust. Nonlinear Seismics. Swirls and Hurricane), Izhevsk: Inst. Komp'yut. Issled., 2010.
- Patalakha, E.I., Lukienko, A.I., and Derbenev, V.A., *Tektonofatsii mezozony* (Tectonofacies of the Mesozone), Alma-Ata: Nauka KazSSR, 1987.
- Petrov, V.A., Role of seismodeformation in the formation of vein–stockworks hydrothermal deposits, *Novye gorizonty v izuchenii protsessov magmo- i rudobrazovaniya: Mater. nauch. konf.* (New Horizons in Studying Magma and Ore Formation. Proceeding of Conference), Moscow: IGEM RAN, 2010, pp. 290–291.

- Petrov, V.A., *Tectonophysical and structural–petrophysical indicators of fluid migration in the fault zones and methods of their study*, *Sovremennaya tektonofizika. Metody i rezultaty (Modern Tectonophysics. Methods and Results)*, Moscow: IFZ RAN, 2011, vol. 2, pp. 94–108.
- Petrov, V.A., Lespinas, M., and Hammer, I., Tectonodynamics of fluid-conducting structural elements and migration of radionuclides in massifs of crystalline rocks, *Geol. Ore Deposits*, 2008, vol. 50, no. 2, pp. 89–111.
- Prokof'ev, V.Y., Bortnikov, N.S., Kovalenker, V.A., Vinokurov, S.F., Zorina, L.D., Chernova, A.D., Kryazhev, S.G., Krasnov, A.N., and Gorbacheva, S.A., The Darasun gold deposit, Eastern Transbaikalian Region: chemical composition, REE patterns, and stable carbon and oxygen isotopes of carbonates from ore veins, *Geol. Ore Deposits*, 2010, vol. 52, no. 2, pp. 91–125.
- Prokof'ev, V.Y. and Pek, A.A., Problems in estimation of the formation depth of hydrothermal Deposits by data on pressure of mineralizing fluids, *Geol. Ore Deposits*, 2015, vol. 57, no. 1, pp. 1–20.
<https://doi.org/10.1134/S1075701515010043>
- Prokofiev, V.Y., Safonov, Y.G., Lüders, V., Borovikov, A.A., Kotov, A.A., Zlobina, T.M., Murashov, K.Y., Yudovskaya, M.A., and Selektor, S.L., The sources of mineralizing fluids of orogenic gold deposits of the Baikal-Patom and Muya areas, Siberia: constraints from the C and N stable isotope compositions of fluid inclusions, *Ore Geol. Rev.*, 2019, vol. 111, 102988.
<https://doi.org/10.1016/j.oregeorev.2019.102988>
- Ramsay, J.G. and Huber, M.I., *The Techniques of Modern Structural Geology*, London: Academ. Press, 1987, vol. 1–2.
- Randall, M.J., Shear invariant and seismic moment for deep-focus earthquakes, *J. Geophys. Res.*, 1971, vol. 76, no. 20, pp. 4091–4092.
- Rastsvetaev, L.M., Influence of paragenetic families of tectonic faults as method of paleogeomechanical analysis of stress and deformation fields in the crust, *Polya napryazhenii i deformatsii v zemnoi kore (Stress and Deformation Fields in the Crust)*, Moscow: Nauka, 1987, pp. 171–181.
- Roedder, E., *Fluid Inclusions* (Mineral. Soc. Amer., Washington, 1984).
- Riedel, W., Zur mechanik geologischer brucherschei-nungen, *Zbl. Mineralogie, Geol. Und Palaentol.*, 1929, vol. B30, pp. 354–368.
- Rytsk, E.Yu., Kovach, V.P., Yarmolyuk, V.V., Kovalenko, V.I., Bogomolov, E.S., and Kotov, A.B., Isotopic structure and evolution of the continental crust in the East Transbaikalian segment of the Central Asian Foldbelt, *Geotectonics*, 2011, vol. 45, no. 5, pp. 349–377.
- Rytsk, E.Yu., Velikoslavinskii, S.D., Alekseev, I.A., Bogomolov, E.S., Kovach, V.P., and Samorukov, V.I., Geology of the Karalon gold ore field in the Mid-Vitim Highlands, *Geol. Ore Deposits*, 2018, vol. 60, no. 4, pp. 300–327.
<https://doi.org/10.1134/S0016777018040044>
- Safonov, Yu.G., Formation depth and distribution of ore deposits, *Otechestvennaya Geol.*, 2000, no. 4, pp. 20–27.
- Sibson, R.H., Fluid flow accompanying faulting: field evidence and models, *Earthquake Prediction: An International Review*, Simpson, D.W., and Richards, P.G., Eds., *Am. Geophys. Union, Maurice Ewing Ser.*, 1981, vol. 4, pp. 593–603.
- Sibson, R.H., Robert, F., and Poulsen, K.H., High-angle reverse faults, fluid pressure cycling, and mesothermal gold-quartz deposits, *Geology*, 1988, vol. 16, pp. 551–555.
[https://doi.org/10.1130/0091-7613\(1988\)016<0551:HARFFP>2.3.CO;2](https://doi.org/10.1130/0091-7613(1988)016<0551:HARFFP>2.3.CO;2)
- Sibson, R.H. and Skott, J., Stress-fault control on the containment and release of overpressured fluids: examples from gold-quartz vein systems in Juneau, Alaska, Victoria, Australia, and Otago, New Zeland, *Ore Geol. Rev.*, 1998, no. 13, pp. 293–306.
[https://doi.org/10.1016/S0169-1368\(97\)00023-1](https://doi.org/10.1016/S0169-1368(97)00023-1)
- Sibson, R.H., Controls on maximum fluid overpressure dating conditions for mesozonal mineralization, *J. Struct. Geol.*, 2004, vol. 26, nos. 6–7, pp. 1127–1136.
<https://doi.org/10.1016/j.jsg.2003.11.003>
- Sim, L.A., Tectonic stresses of the northern Urals and their influence of the formation of rock crystal pockets, *Osnovnye problemy v uchenii ob endogennykh rudnykh mestorozhdeniyakh: novye gorizonty: Mater. Vseros. Konf (Main Problems in Theory of Endogenous Ore Deposits: New Horizons. Proc. All-Russian Conference)*, Moscow: IGEM RAN, 2017, pp. 189–192.
- Sylvester, A.G., Strike-slip faults, *Geol. Soc. Am. Bull.*, 1988, vol. 100, no. 11, pp. 1666–1703.
[https://doi.org/10.1130/0016-7606\(1988\)100<1666:SSF>2.3.co;2](https://doi.org/10.1130/0016-7606(1988)100<1666:SSF>2.3.co;2)
- Vertlib, M.B., Earthquake hypocenters and mechanism in relation with geodynamics of northeastern Baikal Zone, *Geofiz.*, 1997, vol. 38, no. 8, pp. 1376–1385.
- Vidal, O., Baldeyrou, A., Dubac, B., De'Andrade, V., Jullien, M., and Lanson, B., Thermodynamics of phyllosilicates and low temperature thermometry., *Diagenesis and Low-Temperature Metamorphism. Theory, Methods and Regional Aspects. Seminarios de la Sociedad Espanola de Mineralogia*, Nieto, F. and Jimenez-Millan, J., Eds., 2007, vol. 3.
- Vikent'eva, O.V., N.S. Bortnikov, I.V. Vikentyev, E.O. Groznova, Lyubimtseva, N.G., and Murzin, V.V., The Berezovsk giant intrusion-related gold quartz deposit, urals, russia: evidence for multiple magmatic and metamorphic fluid reservoirs, *Ore Geol. Rev.*, 2017, vol. 91, pp. 837–863.
- Woodcock, N.H. and Fischer, M., Strike-slip duplexes, *J. Struct. Geol.*, 1986, vol. 8, no. 7, pp. 725–735.
- Yunga, S.L., Classification of seismic moment tensors on the basis of their isometric mapping on a sphere, *Dokl. Earth Sci.*, 1997, vol. 352, no. 2, pp. 108–110.
- Zlobin, T.K., *Stroenie zemnoi kory i verkhnei mantii Kuril'skoi ostrovnoidi dugi (po seismicheskim dannym)* (Structure of the Earth's Crust and Upper Mantle beneath the Kuril Island Arc from Seismic Data), Vladivostok: DVNTs AN SSSR, 1987. 150 s.
- Zlobina, T.M., *Matematicheskie metody modelirovaniya treshchinnykh struktur rudnykh mestorozhdenii* (Mathematic Methods of Modeling the Fracture Structures of Ore Deposits), Moscow: Nauka, 1991.
- Zlobina, T.M., Petrov, V.A., Prokof'ev, V.Y., Kotov, A.A., and Murashov, K.Yu., Influence of headwater fluid-saturated fluids on the stress-deformation medium of the formation of orogenic gold deposits, *Triggernye efekty v geosistemakh: Mater. IV Vseros. konf (Trigger Effects in Geosystems. Proc. 4th All-Russian Conference)*, Adushkin, V.V. and Kocharyan, G.G., Eds., Moscow: GEOS, 2017, pp. 274–284.
- Zlobina, T.M., Petrov, V.A., Prokofiev, V.Y., Kotov, A.A., Murashov, K.Yu., Wolfson, A.A. The Uryakh ore field (NE Transbaikalia): formation of structural assemblages in the centroid-type seismic regime, *Dokl. Earth Sci.*, 2016, vol. 470, no. 2, pp. 1050–1055.
<https://doi.org/10.1134/S1028334X16080195>